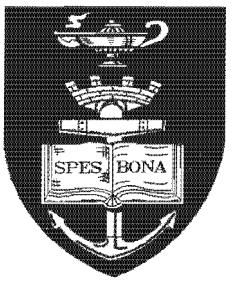

The Neutralisation of Acid Mine Drainage by Fly Ash

R.D. O'Brien

Submitted in partial fulfilment of the
requirements for the degree of
Master of Science in Environmental Geochemistry
In the Department of Geological Sciences
University of Cape Town
January, 2000

Abstract

South Africa is largely dependent of the combustion of coal for power generation. Approximately 22 Mt of ash was produced in 1999 by ESKOM, the largest producer of electricity in South Africa. Of this only 1.1 Mt was utilised, the rest being disposed of in landfills or ash dams. Various environmental impacts are associated with the disposal of fly ash including loss of usable land, dust pollution, water pollution, effects on vegetation and aesthetic impacts.

The oxidation of pyrite exposed during the mining of coal results in the generation of large quantities of acid water with a high dissolved metal load. Current legislation requires this water to be collected and neutralised before being discharged. The costs involved in neutralising this effluent and safe storage of the resulting sludge can be enormous.

In South Africa the power stations are built adjacent to the colliery which supplies the coal. This results in a unique situation where two waste stream of contrasting character are situated in close proximity to each other. The aim of this study is to investigate the reactions of acid mine drainage (AMD) and fly ash in order to evaluate the potential for their co–disposal.

A simulated AMD containing 364 mg/l Al, 355 mg/l Fe, 2782 mg/l SO_4^{2-} as the major ions at pH 2.5 was prepared and used in all experiments. Fresh fly ash was collected from the Arnot power station and from Sasol. The mineralogy of the two fly ashes is similar. The mineralogical phases present in the fly ash are glass, quartz and mullite with accessory lime and hematite. Sasol fly ash has a lower lime and higher mullite concentration than the Arnot fly ash. The concentration of quartz is similar in the two ashes. The differences in the mineralogy of the fly ashes is reflected in their chemical composition, with the Sasol ash having a lower concentration of CaO (5.4 wt%) compared to 7.3 wt% in the Arnot fly ash. The Al_2O_3 concentration in the Sasol ash is higher (29.9 wt%) than the Arnot fly ash (22.1 wt%). The morphology of the Arnot fly ash is dominated by well rounded glass particles and spheres, indicating a high degree of melting in the furnace. The Sasol fly ash is dominated by blocky particles with a highly irregular morphology. This indicates higher melting temperatures as would be expected due to the lower CaO concentration.

Batch neutralisation experiments were conducted with a series of fly ash: AMD ratios,

and equilibrated on a reciprocating shaker for 72 hours. The results showed that the higher lime concentration of the Arnot fly ash results in a higher neutralisation potential than the Sasol fly ash. The titration curves of AMD and fly ash for the two ash samples have similar shapes, indicating that the neutralisation reactions are the same for both fly ash samples. The titration curves are characterised by four distinct regions. Mineralogical analysis by XRD and SEM and thermodynamic modelling of the solution chemistry enabled the identification of the mineral phases controlling the solution composition. At high pH values (>12.7) the solutions are in equilibrium with portlandite ($Ca(OH)_2$). Between pH values of 12 and 10.3, ettringite ($Ca_6Al_2(SO_4)_3(OH)_{12}\cdot 26H_2O$) precipitates and acts as a weak pH buffer. Below pH 10.3 ettringite dissolves incongruently to form gypsum and amorphous $Al(OH)_3$. Gypsum was identified by XRD to pH values of 5.6, although thermodynamic modelling indicates that the solution is in equilibrium with gypsum to pH value of 4.1. The presence of amorphous $Al(OH)_3$ could not be confirmed directly, but is inferred from the modelling of the solution chemistry. Very little buffering is observed between pH values of 10.3 and 4.5, where the solution composition is controlled by gypsum and amorphous $Al(OH)_3$. Between pH values of 4.5 and 4.1 the system exibits a very strong buffering capacity, which is considered to be the result of the dissolution of the amorphous $Al(OH)_3$.

The mineralogy of the iron precipitates was identified by means of XRD to be 2 line ferrihydrite. SEM examination of the reacted fly ashes showed the ferrihydrite to form coatings on the fly ash particles.

The kinetics of the neutralisation reactions were investigated by monitoring the pH and electrical conductivity (EC) of three fly ash: AMD mixtures (1:5, 1:10, 1:20) over a period of 72 hours. The kinetics of the neutralisation reactions are initially very rapid, with the pH increasing from 2.5 to 4 within 5 minutes for all fly ash: AMD ratios. This rapid neutralisation reaction is considered to be the result of the free lime present in the fly ash. The reaction rates decrease as equilibrium is approached. For both fly ash samples the pH had stabilised within 24 hours. Those experiments whose equilibrium pH was below pH 10 maintained a constant EC from the time the pH stabilised until the experiment was terminated. Where the equilibrium pH was higher than 10 the EC continued to decrease and had not stabilised when the experiments were ended. This slow decrease in the EC is considered to be due to the slower

kinetics of ettringite precipitation as equilibrium is approached.

The co-disposal of AMD and fly ash shows potential as a means of neutralising the extreme pH of these waste streams. The Arnot fly ash has a greater neutralisation potential than the Sasol fly ash.

Table of Contents

List of Figures

List of Tables

Abreviations and acronyms

AMD	Acid mine drainage
EC	Electrical conductivity
EDXRF	Energy dispersive X-ray fluorescence spectroscopy
FTIR	Fourier transform infrared spectroscopy
HPIC	High pressure liquid chromatography
ICP-MS	Inductively coupled plasma mass spectroscopy
LOI	Loss on ignition
PFA	Pulverised fuel ash
SEM	Scanning electron microscopy
SI	Saturation index
XRD	X-ray diffractometry
XRF	X-ray fluorescence spectroscopy

Chapter 1: Introduction

ESKOM is the largest producer of electricity in South Africa and produced 21.8 Mt of fly ash in 1997. Of the 21.8 Mt of ash produced 1.114 Mt was sold (ESKOM, 1999), the rest being disposed of in landfills or ash dams. With increasing industrialisation and population growth the demand for cheap energy sources will continue to grow. South Africa, with its vast coal reserves, relies heavily on coal fired power stations for electricity generation. Various environmental impacts are associated with the disposal of fly ash including loss of usable land, dust pollution, water pollution, effects on vegetation and aesthetic impacts (Smith and Harris, 1987).

Acid mine drainage (AMD) is formed by the oxidation of sulfide minerals, particularly pyrite, when exposed to oxygen and water. During the mining and beneficiation of coal, large quantities of pyrite are brought into contact with water and oxygen, often resulting in the generation of AMD. The metal load of these acid waters depends on the mineralogy of the host rocks and is typically dominated by iron and aluminium.

As the demand for coal increases, for local electricity production or export, the volumes of AMD generated are likely to increase. Current environment legislation requires this water to be collected and neutralised before being discharged. A range of chemical treatment options is available for the neutralisation of AMD. These include the addition of lime, limestone, sodium carbonate or sodium hydroxide (Pulles *et al.*, 1996). The most commonly used neutralising agent is lime, which is usually added in the form of slaked lime. While the financial costs involved in neutralising this effluent and safe storage of the resulting sludge can be enormous, the contamination and loss of usable water in a water poor country could be even higher.

In South Africa the power stations are built adjacent to the colliery which supplies it with coal. This results in a situation where two waste streams of contrasting character are in close proximity to each other. This unique situation prompted the initiation of this study. Although a number of studies have been made investigating the potential of fly ash to prevent the generation of AMD in coal mines, no studies could be found in the literature involving the neutralisation of AMD by fly ash. The results of these studies have been mixed, with the kinetics of AMD generation and fly ash leaching playing a major role.

The objectives of this study were to investigate the potential for the co-disposal of fly ash and AMD by:

- characterising the mineralogy and chemistry of two South African fly ashes with respect to their potential as liming agents.
- investigate the mineralogy of the precipitates formed during the neutralisation reactions.
- investigate the solution chemistry and identify the minerals controlling the solution composition.
- examine the kinetics of the neutralisation reactions.

This thesis consists of three main sections starting with a review of the recent literature dealing with the neutralisation of AMD and fly ash mineralogy and chemistry. The second section is allocated to the results and discussion of the chemical and mineralogical characteristics of the fly ash samples, the mineralogy of the precipitates, solution chemistry and kinetics, followed by a chapter on the conclusions to this study.

Chapter 2: The neutralisation of acid mine drainage and geochemistry of fly ash. A literature review.

2.1 Introduction

Acid mine drainage (AMD) is the single most important source of water contamination in the coal mining industry. The effects of AMD on the environment can be severe, leading to the absence of life in receiving waters. The current legislation (Water Act 54 of 1956) requires the minerals industry to treat their wastewater before releasing it to receiving water bodies. A range of potential remediation strategies is available depending on the quality of the wastewater.

Pulverised fuel ash (PFA) is the solid waste product resulting from coal combustion during power generation. The extensive use of coal for electricity generation in South Africa produced 21.8 million tons of PFA during 1999 (ESKOM, 1999). In addition the petrochemical company Sasol produced 11.97 Mt of ash during the 1998 (Sasol, 1998). This fly ash is currently disposed of in landfills and in ash dams. The environmental effects of fly ash are the result of its relatively unstable mineralogy, which upon weathering results in a leachate with high pH, hardness and TDS. In addition the fly ash contains high concentrations of potentially toxic elements, such as B, Mo, As and Se, which can be released to the environment upon weathering (Adriano *et al.*, 1980).

The purpose of this literature review is to assess the current state of knowledge with regards to the neutralisation of AMD and weathering of fly ash with the aim of assessing the potential utilisation of fly ash as an alternative liming agent.

2.2 The Chemical and Mineralogical Properties of Fly Ash

The chemistry and mineralogy of fly ash is determined by a number of factors, including the composition of the coal, conditions in the combustion chamber, type of emission control devices and the disposal methods used. Willis (1987) found significant variations in the composition of South African fly ash. These variations reflect the differences in the parent coal composition from different coalfields and coal seams.

Fly ash consists predominantly of glass spheres ranging from 0.01 to 100 μm in size. The spheres include solid glass spheres, hollow glass spheres (cenospheres) and

hollow glass spheres containing other glass spheres (plerospheres).

The most common minerals found in fly ash are quartz and mullite ($Al_6Si_2O_{13}$) with lesser amounts of magnetite, maghemite, anhydrite and lime (Bezuidenhout, 1995). Warren and Dudas (1984) found sub micron sized CaO fragments on the surface of the glass spheres.

Mullite is formed by the decomposition of aluminosilicate phases in the coal. The most common aluminosilicate mineral in coal is kaolinite, which decomposes to mullite according to reactions 10 and 11 (White and Case, 1990).

$$\underset{\text{kaolinite}}{Al_2O_3 \cdot 2SiO_2 \cdot 2H_2O} \xrightarrow{500^\circ C} \underset{\text{metakaolin}}{Al_2O_3 \cdot 2SiO_2} + 2H_2O \qquad (1)$$

$$\underset{\text{metakaolin}}{3(Al_2O_3 \cdot 2SiO_2)} \xrightarrow{980^\circ C} \underset{\text{mullite}}{3Al_2O_3 \cdot 2SiO_2} + 4SiO_2 \qquad (2)$$

Warren and Dudas (1984) conducted a series of column leaching experiments of fly ash to evaluate the relationship between leachate properties, weathering processes and the fly ash solid phase. They found that the initial leachate was dominated by high concentrations of Ca, Na, and K, and high pH is related to the dissolution of the CaO fragments and highly soluble surface salts. They concluded that the high initial pH was the result of the hydrolysis of CaO and subsequent dissolution of $Ca(OH)_2$.

2.3 The Origin of Acid Mine Drainage

Acid mine drainage can be formed wherever sulfide containing rock is exposed to air and water. The sulfides within these rocks are oxidised releasing acid to the water. Although all sulfide minerals can potentially form acid mine drainage, the iron sulfide, pyrite, is the major acid generating sulfide mineral in South Africa (Pulles *et al.*, 1996).

The oxidation of pyrite, FeS_2, is a complex sequence of chemical, biological and electrochemical reactions. The initial oxidation of pyrite by O_2, reaction (3), results in the release of ferrous iron and sulphate together with acidity (Singer and Stumm, 1970). Following the initial oxidation reaction a sequence is established whereby the ferrous iron is oxidised to ferric iron (reaction 4). This ferric iron is then reduced by pyrite, producing more ferrous iron and acidity (reaction 5). The oxidation of Fe^{2+} to Fe^{3+} (reaction 4) is pH dependent and proceeds slowly at the pH typically encountered during AMD formation, pH <4.5. At low pH, ferric iron oxidises pyrite

(reaction 5) more rapidly than O_2 and more rapidly than the oxidation of Fe^{2+} by O_2 (Singer and Stumm, 1970). Reaction 4 is, therefore, considered to be the rate determining reaction in acid mine drainage generation. The rate of reaction 4 is greatly accelerated by iron-oxidising bacteria such as *Thiobacillus ferrooxidans.* These bacteria can increase the rate of Fe^{2+} oxidation by 5 to 6 orders of magnitude (Nordstrom *et al.*, 1979). *T. ferrooxidans* is an acidophillic bacteria that is common in geological environments containing pyrite. These bacteria are most active from pH 1.0 to 3.5, and can exist in the pH range 0.5 to 6 (Pulles *et al.*, 1996; Bigham *et al.*, 1996).

$$FeS_2 + 7/2\,O_2 + H_2O \Rightarrow Fe^{2+} + 2\,SO_4^{2-} + 2\,H^+ \qquad (3)$$

$$Fe^{2+} + 1/4\,O_{2(aq)} + H^+ \Rightarrow Fe^{3+} + 1/2\,O_2 \qquad (4)$$

$$FeS_2 + 14\,Fe^{3+} + 8\,H_2O \Rightarrow 15\,Fe^{2+} + 2\,SO_4^{2-} + 16\,H^+ \qquad (5)$$

$$Fe^{3+} + 3\,H_2O \Rightarrow Fe(OH)_{3(s)} + 3\,H^+ \qquad (6)$$

The acidic water formed by sulfide oxidation may react with other minerals in the rocks along the flow path. While these reactions can neutralise some of the acidity, they can also introduce potentially toxic elements to the acid mine drainage.

2.4 The Chemistry and Mineralogy of Acid Mine Drainage

Acid mine drainage is a multi-factor pollutant. The low pH of AMD is an intensity factor and a measure of the activity of the hydrogen ion in solution. The acidity of AMD refers to its ability to buffer changes in pH following the addition of a strong base. The acidity of AMD results from the hydrolysis of Fe^{3+} and Al^{3+}. The pH of AMD controls many of the dissolution/precipitation reactions and can result in elevated concentrations of toxic elements in AMD. The pH also affects the oxidation of Fe^{2+} and Fe^{3+} (Singer and Stumm, 1970). Acid mine drainage can be considered to be a low pH solution of ferrous sulphate. The pH values reported in the literature vary considerably, but values as low as 2 are common.

The mineralogy of precipitates from AMD has been shown by Bigham *et al.* (1992) to be a function of pH. At a pH > 4.3 ferric hydroxide precipitates and aluminium hydroxides precipitate above pH 5.2. At a pH of 3 and below the formation of ferric iron minerals must be mediated by micro-organisms (Schwertmann and Fitzpatrick, 1992)

The most common iron minerals in AMD precipitates are goethite (α-FeO(OH)), ferrihydrite ($5Fe_2O_3 \cdot 9H_2O$) and jarosite ($KFe_3(SO_4)_2(OH)_6$) (Jambor, 1994). The precipitation of jarosite from acid ferrous sulphate solutions has been studied by Stahl et al. (1993). They found that the precipitation of jarosite is slower than that of goethite and that the kinetically controlled metastable equilibria between these minerals may control their formation rather than true thermodynamic equilibrium. Karathanasis et al. (1988) found that soil solutions and surface waters contaminated by AMD were supersaturated with respect to jarosite. The levels of soluble Fe^{3+} in these solutions were, however, consistent with the stoichiometry of jarosite indicating kinetic control or the presence of an iron phase with a similar stoichiometry to jarosite but with the higher solubility.

Nordstrom (1982) has shown that the basic aluminium sulphate minerals, jurbanite ($Al(SO_4)(OH) \cdot 5H_2O$), alunite ($KAl_3(SO_4)_2(OH)_6$) and amorphous aluminium sulphates, control the solution concentration of Al^{3+} below pH 4.5. Similar results were reported by Karathanasis et al. (1988) who found that the high aluminium concentrations of soil solutions associated with acid mine watersheds were controlled by the basic aluminium sulphate minerals jurbanite and alunite, and not by gibbsite or kaolinite.

2.5 The Neutralisation of Acid Mine Drainage

The neutralisation of AMD is the process whereby the pH of the water is raised towards a neutral pH of 7. Although the pH standard for general effluent release to the environment is between 5.5 to 9.5, the standards for water reuse in industrial applications such as cooling water and steam generation are much stricter. The neutralisation strategy employed must also reduce the concentrations of sulphate, iron and other metals in the treated water.

The neutralisation of AMD is commonly achieved by chemical additions. The most commonly used chemicals are CaO, $Ca(OH)_2$, $CaCO_3$, NaOH and Na_2CO_3 (Pulles *et al.*, 1996; Hedin *et al.*, 1994). The use of NaOH and $NaCO_3$ has generally been limited due their high cost and the high total dissolved salt (TDS) concentration of the neutralised water. While CaO, $Ca(OH)_2$ and $CaCO_3$ are less reactive than the sodium salts they achieve a greater attenuation of the sulphate concentration in the treated water.

2.5.1 Liming

The neutralisation of AMD is most commonly achieved by the addition of hydrated lime ($Ca(OH)_2$). The lime is usually mixed with water to form a slurry, which is then added to the AMD. Many mines in South Africa have installed automatic dosing systems with feedback from pH probes (Pulles *et al.*, 1996). The major disadvantages of using lime as a neutralisation agent is the low solubility and the lack of any residual alkalinity after treatment. The low solubility can cause problems with automatic dosing systems as slow reaction times lead to overdosing. The reactions involved in neutralising AMD are as given by Thompson (1980):

$$H_2SO_4 + Ca(OH)_2 \Rightarrow CaSO_4(s) + 2H_2O \qquad (7)$$

As the pH is raised, Fe^{3+} and Al^{3+} precipitate as hydroxides. The precipitation of these hydroxides releases some acidity (reaction 6), which acts as a pH buffering the system at pH 3 and pH 4 respectively.

2.5.2 Limestone Drains

The use of limestone ($CaCO_3$) for the neutralisation of AMD is increasing. The benefits of $CaCO_3$ are its slightly lower cost relative to lime and that it can impart a bicarbonate buffer capacity to the water. The major drawback of $CaCO_3$ is the slow reaction rate. The neutralisation reactions involving $CaCO_3$ are dependent on the pH of the water, as given below (Blowes *et al.*, 1998).

$$CaCO_{3(s)} \Rightarrow Ca^{2+} + CO_3^{2-} \qquad pH > 10.3 \qquad (8)$$

$$CaCO_{3(s)} + H^+ \Rightarrow Ca^{2+} + HCO_3^- \qquad 10.3 < pH > 6.3 \qquad (9)$$

$$CaCO_{3(s)} + 2H^+ \Rightarrow Ca^{2+} + H_2CO_{3(aq)} \qquad pH < 6.3 \qquad (10)$$

$$H_2CO_{3(aq)} \Leftrightarrow H_2O + CO_{2(g)} \qquad (11)$$

At pH 6.3 and above the reaction (9) produces HCO_3^-, while below pH 6.3 the reaction (10) produces H_2CO_3. The carbonic acid formed in reaction 10 will dissociate according to reaction 11, releasing CO_2.

The slow reaction rate and low cost of $CaCO_3$ has led to the development of passive systems to neutralise AMD. These systems consist of large drains filled with crushed limestone through which the AMD flows before being released into a wetland system. The increasing pH and oxidation of Fe^{2+} in the drains results in the precipitation of

$Fe(OH)_3$, which coats the limestone (armouring) and prevents any further neutralisation reactions from taking place (Hedin *et al.*, 1994; Gazea *et al.*, 1996). The problems of armouring led to the development of anoxic limestone drains (ALD). Anoxic limestone drains are buried under a layer of clay, typically with a plastic liner above the limestone to prevent the exchange of evolved CO_2 and atmospheric O_2. The high P_{CO2} generated in the ALD enhances the alkalinity generating potential of the ALD by increasing the equilibrium concentrations of alkalinity and the rate of calcite dissolution (Hedin *et al.*, 1994). The alkalinity generated by an ALD can be as high 300mg/L, which serves as a buffer for the acidity generated by hydrolysis of Fe^{3+} once the water is discharged from the drain. Although the use of ALD looks promising, results from field trials show that current designs are only effective if used to treat AMD with low concentrations of Fe^{3+} (>2 mg/L), Al^{3+} (>2 mg/L) and dissolved oxygen (>1 mg/L) (Gazea *et al.*, 1996).

Ziemkiewicz et al. (1997) have shown that the effects of armouring can be overcome if built into the design of aerobic limestone drains. The results of their laboratory studies indicate that armouring reduced the effectiveness of limestone by 2% at pH 4 and by 45% at lower pH. The field trials of aerobic limestone drains indicate that the effects of armouring can be reduced if the drain is constructed on a steep slope (> 20%). This requirement necessitates the construction of very large, long drains to maintain the retention time of the AMD.

2.5.3 Other Neutralising Agents

Na_2CO_3 and NaOH have much higher solubilities than the corresponding calcium chemicals. They are, however, very expensive and are not used to neutralise AMD on a large scale. They do have a distinct advantage in that they do not increase the Ca concentration of the water and are well suited to neutralise AMD where the water is to be recycled.

2.5.4 Fly Ash

Few studies have been conducted investigating the potential of fly ash as a liming agent for the neutralisation of AMD. The codisposal of fly ash with coal mining spoil having an acid generating potential has been investigated by Stewart *et al.* (1997). In this study column leaching experiments ran for a period of 4 years. The results showed that fly ash was successful in maintaining the pH of the leachate between 7 and 8 for the duration of the experiment. The column leaching experiments of

Warren and Dudas (1984) used a 0.005 mol/L H_2SO_4 eluant to simulate weathering of fly ash. The results of these experiments showed the presence of two buffering reactions by the fly ash. The first buffer at pH 12 was associated with the hydrolysis and dissolution of $Ca(OH)_2$. The second buffering reaction occurred at pH 10 and decreased slowly to pH 8.5 to 9.0. This buffer is associated with the dissolution of the glass phase and resulted in an increase in the concentrations of Si, Fe and Al in the leachate. The changes in the buffer pH from pH 10 to 8.5 - 9.0 were interpreted as being the result of two glass phases with different solubilities.

2.6 Conclusions

The neutralisation of AMD should raise the pH to approximately neutral values while simultaneously causing the precipitation of secondary solid phases. The solid phases should preferably have low solubilities and be stable in the weathering environment.

The small particle size of fly ash and the presence of sub micron sized CaO particles on the surface of glass spheres should make fly ash an extremely reactive neutralising agent. The small particle size and resulting large surface area of the fly ash is expected to reduce the adverse effects of armouring.

Chapter 3: Materials and methods

3.1. Sampling

Arnot fly ash was collected from the base of the electrostatic precipitators into a steel tube and after cooling transferred to two 5 litre plastic buckets with tight fitting lids. To further minimise the formation of calcite in the fly ash the buckets were placed in heavy-duty plastic bags, which were sealed after excluding as much air as possible. Fly ash from the Sasol power station at Sasolburg was collected under the supervision of Martin Ginster, and stored in the same type of plastic bucket as used for the Arnot fly ash. The fly ash was kept in the plastic buckets for the duration of the study. Care was taken to ensure that the lids were sealed at all times.

The rationale for minimising the formation of calcite in the fly ash samples was to ensure that the mineralogy of the ash remained constant for the duration of the study. Secondly although calcite is expexted to be present in fly ash dams, the ingres of CO_2 into a freshly deposited ash waste slurry is expected to be slow, and very little calcite is expected to be present if AMD was codisposed with a fresh fly ash slurry.

3.2. Simulated acid mine drainage

Simulated AMD was prepared using the acid salts and quantities listed in Table 3.1. The aluminium, ferrous and calcium sulphates were dissolved in approximately 1.5 litres of distilled water. In order to minimise the precipitation of ferric hydroxides the pH was lowered to less than 3 by the addition of 2mL 1N H_2SO_4 prior to the addition of the ferric chloride. The solution was then made up to 2 litres. The composition of the simulated AMD is given in Table 3.2. The concentrations of total and ferrous iron were determined by colorimetry according to standard method 3500-Fe D (Standard Methods, 1995), with ferric iron calculated by difference. All other concentrations are calculated from the respective molecular weights.

Table 3.1: Reagents used to make up 1 litre of simulated AMD.

Chemical	Mass (g)	Supplier
$Al_2(SO_4)_3 18H_2O$	4.50	Merck N.T
$FeSO_4 7H_2O$	3.00	Merck
$CaSO_4 2H_2O$	0.80	Merck
$FeCl_3 6H_2O$	0.60	Saarchem
H_2SO_4 (1N)	2.00 mL	

The composition of the simulated AMD was based on the analyses of waters of the Blesbokspruit catchment reported in the work of Hälbich (1997). The acid waters of this area are highly variable in composition. The analyses of two waters from this area are presented with that of the simulated AMD in Table for comparison. Sample T2 (DWAF, 1985 as cited in Hälbich, 1997, p.3-5) is a borehole water sample adjecent to the Travistock Colliery and sample W7 (Hälbich, 1997, p.4-17) is a surface water taken from an AMD collection dam at the Witbank colliery.

Table 3.2: Composition of simulated AMD and acid mine waters from the Blesbokspruit catchment.

	Simulated AMD	W7	T2
pH	2.6	2.7	2.9
EC (mS/cm)	3.35	3.63	3.68
Al^{3+} (mg/L)	364.4	190	38
Ca^{2+}	117.8	136	462
Fe^{2+}	276.7		
Fe^{3+}	84.9		
Fe_{total}	361.7	34.6	726
Cl^-	95.9	363	4.8
SO_4^{2-}	2782	1509	3840

3.3. Experimental procedures

3.3.1. Batch neutralisation experiments

The mutual neutralisation of AMD and fly ash was investigated by conducting a batch style experiment. Different amounts of fly ash were weighed out into a series of polypropylene containers to which the simulated AMD was added to yield ash: AMD ratios of 1:5, 1:10, 1:15, 1:20, 1:25, 1:30, 1:35, 1:40 and 1:50. The containers were sealed and placed on a reciprocating shaker and shaken at a constant speed for 72 hours. The time of 72 hours was selected based on the results of kinetic experiment as being sufficient for the pH to stabilise.

After 72 hours the containers were removed from the shaker and the samples were filtered through a 0.45 μm Millipore filter. The pH and EC of all filtrates was measured immediately after filtration. Each filtrate was divided into 2 sub samples, one of which was acidified with 2mL of concentrated HCl per 100 mL of sample. The

solutions were kept refrigerated at approximately 4°C. Total and ferrous iron was determined by colorimetry using the acidified solutions. Aluminium and Si were analysed by ICP-MS, while the anions and remaining major cations were analysed by IC, on the unacidified samples.

The remaining ash was rinsed with a small amount of distilled water followed by a rinsing in ethanol, filtered and allowed to air dry. In order to investigate the mineralogy of the secondary precipitates the <63μm fraction was separated by wet sieving in alcohol. The <63μm fraction was then concentrated by centrifuging, mounted on a glass slide and analysed by XRD. This procedure did not provide a satisfactory diffraction pattern, as the concentration of the secondary precipitates was not high enough to be clearly discernible above the background of the glass spheres.

It was then decided to separate a finer size fraction by sedimentation in alcohol. The samples were mixed with approximately 15 mL of ethanol and dispersed using an ultrasonic probe. The dispersed sample was transferred to a glass cylinder and shaken vigorously. After 65 minutes the upper 10 cm of solution was removed with a pipette. This size fraction would have a hydraulic equivalent diameter of less than <5 μm. The solids were concentrated by centrifuging for 5 minutes at 6000 r.p.m. The supernatant was discarded and the sediment transferred with a pasteur pipette to a glass slide and allowed to air dry. The <5μm fraction was selected as it allowed sufficient sample recovery to coat a glass slide for XRD analysis.

The experiment was also performed using distilled water as a control although only the pH and EC of the filtrate was measured.

3.3.2. Kinetic experiments

The kinetics of the neutralisation reactions were investigated using 3 ratios of fly ash to AMD (1:5, 1:10 and 1:20), for both the Arnot and Sasol fly ash. The procedure followed was to weigh out 1, 2 and 4 grams of fly ash into a series of polypropylene centrifuge tubes to which 20 mL of simulated AMD was added. The centrifuge tubes were sealed and then placed on a reciprocating shaker. After time intervals of 5, 15, 30 and 60 minutes and 2, 4, 6, 8, 12, 24, 48 and 72 hours a centrifuge tube was removed from the shaker. After removing the centrifuge tube from the shaker, the sample was centrifuged at 4000 rpm for 3 minutes. The pH and EC were measured in the supernatant immediately after centrifuging to minimise contact with

atmospheric CO_2. The experiment was conducted at the ambient temperature, which varied from 15 to 21°C.

Randomly selected runs were repeated during the course of the experiment, but at different times of the day. A comparison of these duplicates revealed that the results were reproducible for runs which lasted longer than 24 hours. The duplicates of the short term runs were not reproducible. The measurement time and experimental time of the short term runs are comparable, This will introduce larger uncertainties in the data than in the long term runs. Changes in the ambient temperature will also introduce larger uncertainties at the low times compared to the longer running experiments.

3.3.3. AMD fly ash extracts

Saturated paste extracts of fresh fly ash from both sources were prepared according to the method of Rhoades (1982). Two 400g samples of each ash were weighed into a 500 mL polypropylene container and 200 mL of distilled water was added. The containers were closed and sealed with parafilm to prevent any CO_2 ingress. The pastes were allowed to equilibrate for a period of 24 hours.

Prior to the extraction, 30 mL of distilled water was added to return the paste to a saturated condition. The saturated paste was filtered through Whatman no. 50 filter paper on a Buchner funnel. During filtration the Buchner funnel was tapped continuously to improve the extraction efficiency. The two extracts were combined and stored in a 500 mL polypropylene bottle at 4°C. Approximately 50% of the water added was recovered by this procedure.

The experimental procedure followed was to pipette 10mL of the saturated paste extract into a beaker. A magnetic bar was added and the beaker was placed on a magnetic stirrer. The pH was monitored continuously using a Radiometer model TTT88 titrator. The AMD was added from a glass burette at a rate of approximately 1mL per minute. The fly ash extract was titrated to pH end points of 4 through to 12. At each pH end point the titration was stopped once the pH had remained within 0.01 pH unit for 30 seconds.

On completion of each titration the solution was filtered through a 0.45mm filter. The filtrate was rinsed twice with approximately 5 mL of distilled water and then allowed to air dry. These filtrates were then analysed by FTIR. Three of the titrations, to pH

11, 8 and 5, were repeated using 50mL of the fly ash extracts. This allowed a sufficient amount of the precipitates to be collected for XRD analysis.

3.3.4. Thermodynamic modelling

All thermodynamic calculations were performed using the computer code PHREEQC (Parkhurst, 1995) utilising the MINTEQA2 thermodynamic database (Allison *et al.*, 1991) and the Davies equation for the calculation of the activity coefficients.

The saturation index is an index used to describe the extent to which a particular solution is undersaturated or supersaturated with respect to a particular solid (Drever, 1997). When a solid is in equilibrium with the surrounding solution the ion activity product (IAP) is equal to the solubility product of that solid. The saturation index (SI) is calculated according to the equation:

$$SI = \text{Log}\frac{IAP}{K_{sp}}$$

A negative saturation index indicates that the solid is undersaturated while a positive SI indicates supersaturation.

3.4. Analytical methods

3.4.1. pH and electrical conductivity

The pH of all solutions was measured using a Crison Micro 2001 pH meter with automatic temperature compensation. The instrument was calibrated using a 2 point calibration at pH 7 and either pH 4 or pH 9.26 buffer solution. A pH 10 buffer solution was used as a reference solution. The standard deviation of a series of measurements over the course of a day was typically better than 0.05 pH units. The pH of the equilibration reaction experiments was measured immediately after centrifuging to minimise contact time with atmospheric CO_2.

The electrical conductivity was measured using a Crison Micro CM 2201 conductivity meter with automatic temperature correction at a reference temperature of 25°C. The instrument was calibrated daily with a 0.01M KCl solution. The calibration of the instrument was checked periodically during the course of the day, and recalibrated regularly, as the instrument was prone to significant drift.

3.4.2. ICP-MS

The determination of Al and Si was performed using a Perkin Elmer model Elan ICP-MS. All samples were filtered through a 0.45μm Millipore cellulose filter prior to dilution. The dilution procedure involved the transfer of 15μL of sample to a 15 mL polyethylene centrifuge tube followed by 50 μL of a Rh internal standard and 14.35 mL of 2% HNO_3. The calibration was performed using a series of standard solutions.

3.4.3. Ion chromatography (IC)

The cations Na^+, NH_4^+, K^+, Mg^{2+} and Ca^{2+} and anions F^-, Cl^-, NO_3^- and SO_4^{2-} were determined by IC using a Dionex series 3000 instrument.

The cations were determined using an IonPac CG12A guard column and a CG12A separator column and 10mM H_2SO_4 as the eluent. The anions were determined using an IonPac AS4A guard column and an AS4 separator column with 3.5mM Na_2CO_3 / 1mM $NaHCO_3$ as eluent.

The samples were diluted prior to analysis to yield an EC of approximately 100 mS/cm, and all samples were passed through a P onguard column. Although this column is designed to remove organic molecules from the sample solution which reduce the life of the separation column it also proved effective at removing iron particles that passed through the 0.45μm Millipore filter.

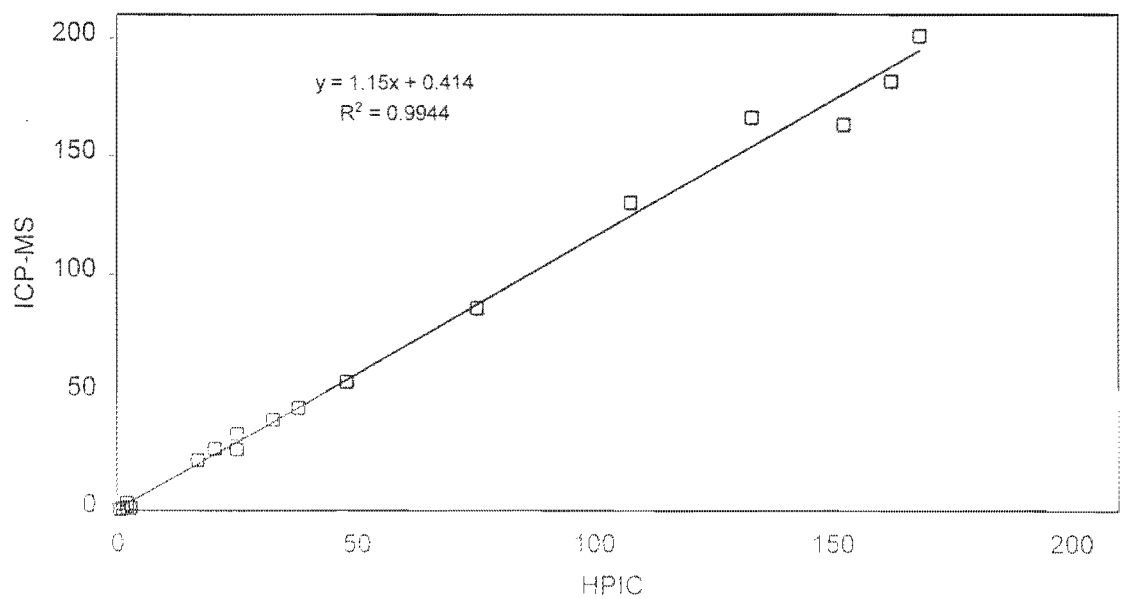

Figure 3.1: The correlation between Mg determined by IC and ICP-MS.

3.4.4. Iron colorimetry

Total and ferrous iron was determined by the phenanthroline method (3500-Fe-D) (Standard methods, 1995). Ferric iron was calculated by difference. Due to the small volume of sample available, the volumes of all reagents in the standard method were halved. Figure 3.2 illustrates the calibration curve obtained using this method.

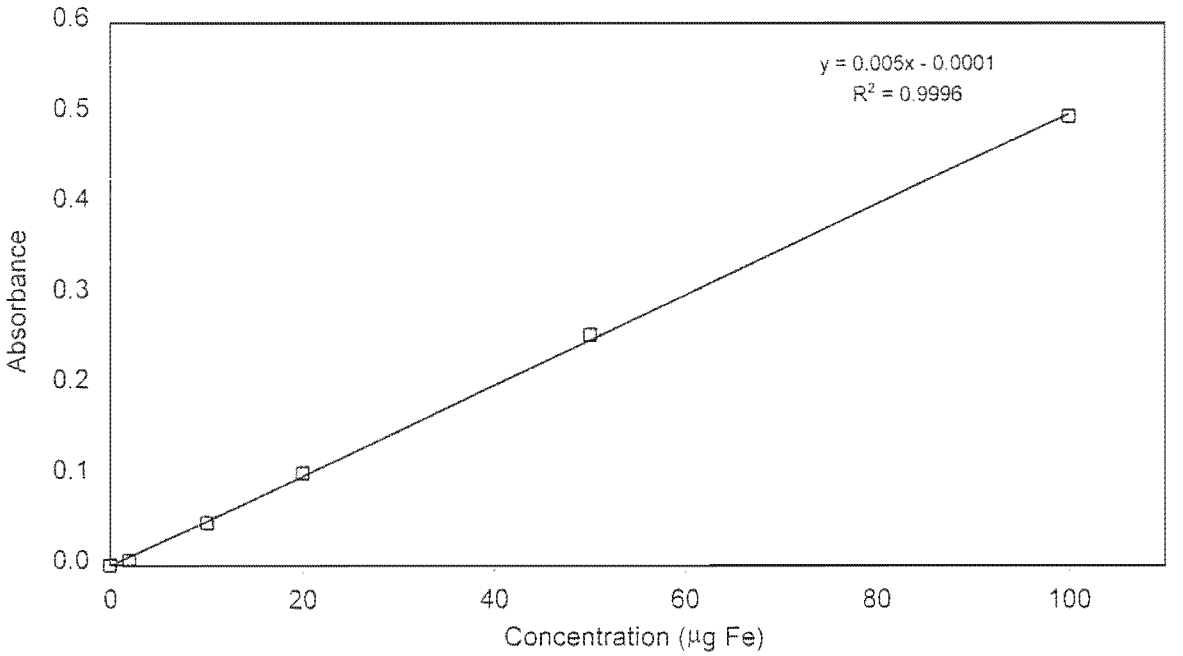

Figure 3.2: Iron calibration curve obtained using the phenanthroline method.

The determination of ferric iron by difference is a function of the accuracy and precision of the ferrous and total iron determinations, especially at very large or small Fe^{2+}/Fe^{3+} ratios (Bangthanh *et al.*, 1999). Bangthanh and co workers (1999) state that the Fe^{2+}/Fe^{3+} ratio should be between 0.2 and 5 for the accurate determination of ferric iron by difference. The Fe^{2+}/Fe^{3+} ratios of the solutions analysed range from 5 to 12, and the calculated ferric iron concentrations should be interpreted with some caution.

3.4.5. X-ray fluorescence spectrometry (XRF)

Approximately 70g of fly ash was ground for 2 minutes in a carbon steel Siebtechnik swing mill. The loss on ignition was determined using a 2g aliquot of the milled fly ash. Adsorbed moisture was determined after 4 hours at 110°C. The loss on ignition was determined gravimetrically after roasting the samples overnight in an Amalgams

muffle furnace at 900°C.

The major and minor elements were determined on fusion discs. The fusion discs were prepared by accurately weighing out 6g of lithium tetraborate / lithium metaborate flux and 0.7g of milled sample. The flux sample mixture was fused using a Claisse–Fluxy fusion disc instrument.

The fusion discs were analysed in the Department of Geological Sciences, UCT on a Phillips PW X'Unique II wavelength dispersive X-ray fluorescence spectrometer. The elemental concentrations are reported as weight percent oxide and corrected for the loss on ignition.

3.4.6. X-ray diffractometry (XRD)

The X-ray diffraction patterns of all samples were collected using a Philips PW 1390 X-ray diffractometer and the Philips X'Pert data collection software. All analyses were conducted using Cu Kα radiation with the tube operated at 40 kV and 25 mA. The sample preparation procedures and scanning parameters were different for each sample type and are discussed below.

The mineralogical composition of the fresh fly ash was determined on an aliquot of sample milled for XRF analysis. The fly ash was back–filled into an aluminium sample holder and pressed against filter paper to prevent any preferred orientation of the mineral grains. The diffraction data was collected from 5 to 60°2θ using a step width of 0.1 °2θ and a counting time of 2 seconds.

The <5μm fractions of the serial titration experiment were prepared on glass slides as described above (3.3.2) and analysed using the same scanning parameters as for the fresh fly ash. The diffraction pattern of a blank glass slide was also collected.

The precipitates of the AMD - fly ash extracts titrations were filtered through a 0.45 μm Millipore filter and air-dried. The precipitate was scraped off the filter with a spatula and ground in a small agate mortar. The samples were packed into a perspex sample holder and pressed with a polished steel die to be flush with the analytical surface. A diffraction pattern of the empty sample holder was obtained as a blank. The diffraction patterns for these precipitates were collected from 5 to 70°2θ using a step width of 0.05°2θ and a counting time of 2.8 seconds. The angular range was extended to 70°2θ to include the broad peak situated at 65°2θ. The step size

was decreased and the counting time increased in order to obtain a sufficiently strong diffraction pattern.

3.4.7. Fourier transform infrared spectroscopy (FTIR)

Fourier transform infrared spectroscopy was performed using KBr disks. Between 2 and 2.5mg of sample was ground in an agate mortar and mixed by grinding with approximately 200mg of KBr. The total grinding time was approximately 5 minutes. The mixture was then pressed in a steel die at 10 tonnes for 1 minute. The die was not evacuated during pressing.

The absorbance spectra were collected using a Paragon 1000 model instrument with a single beam, purgable sample compartment, with a maximum OPD resolution of $1cm^{-1}$. The mid infrared detector was either a DTGS (deuterated triglycine sulphate) or a LITA (lithium tantalate) crystal. The system was controlled by a Motorola 68340 integrated processor. The absorbance spectrum for each sample was obtained by averaging 4 scans over the range 400 to 4000 cm^{-1}.

3.4.8. Scanning electron microscopy (SEM)

Fresh fly ash and the fly ash residues from the batch neutralisation experiments were examined by scanning electron microscopy. The analysis was performed using secondary electrons, backscattered electrons and energy dispersive x-ray spectrometry (SEM EDXRF). A LEICA Stereoscan 440 was used for all analysis. The instrument was operated at a high tension of 15kV and at a working distance of 25mm for all analysis. A beam current of 35pA was employed for the secondary detector and between 700 pA and 1.6 nA for the backscattered electron detector.

The samples were prepared by coating a small aluminium stub with carbon glue and sprinkling the ash onto the stub. Excess sample was removed by gently tapping the stub with a tweezer. The sample was then carbon coated in a sputter coater and stored in an evacuated desiccator until analyses.

Chapter 4: Results and discussion

4.1 Mineralogical and chemical characteristics of fly ash

4.1.1 Fly ash chemistry

The average of duplicate analyses of the major element oxides for both fly ashes are presented in Table 4.1, together with the result from previous studies by Willis (1987) and Campbell (1998). The major differences in the chemical composition of the Arnot and Sasol fly ash are the Al_2O_3, CaO, MgO, Fe_2O_3 content and the loss on ignition (LOI). The Sasol fly ash is characterised by a higher Al_2O_3 content and lower CaO, MgO, Fe_2O_3 and LOI. The higher Al_2O_3 content indicates a higher clay content in the parent coal than that of Arnot. The lower CaO, MgO and Fe_2O_3 concentrations indicate lower concentrations of these elements in the coal, most likely in the form of carbonate minerals.

Table 4.1: The major element composition in weight % of Arnot and Sasol fly ash.

	This study		Willis (1987)		Campbell (1998)
	Arnot	Sasol	Arnot	Sasol	Sasol
SiO_2	53.8 (0.1)#	54.3 (0.4)	53-63	61-67	53.0
TiO_2	1.2 (0.5)	1.6 (1.4)	1.3-1.5	1.2-1.4	1.7
Al_2O_3	22.1 (0.1)	29.9 (0.4)	25-27	23-27	28.5
Fe_2O_3	4.8 (0.3)	3.3 (1.6)	4.8-5.4	3.1-4.8	3.3
MnO	0.05 (3.8)	0.02 (12)	0.4-0.5	0.30	0.04
MgO	2.6 (0.7)	1.0 (0)	1.7-2.0	1.4-1.7	1.4
CaO	7.3 (0.2)	5.4 (0.6)	6.3-7.0	6.1-7.1	6.4
Na_2O	0.07 (18)	0.12 (12)	0.16-0.21	0.76-1.3	0.40
K_2O	0.52 (0.4)	0.51 (0.4)	0.48-0.51	0.31-0.48	0.46
P_2O_5	0.09 (1.5)	0.14 (1.4)	0.38-0.89	0.22-0.51	0.26
SO_3	0.29 (1.8)	0.24 (4.7)	0.15-0.34	0.11-0.26	0.29
LOI	6.5 (0.4)	3.0 (1.4)			4.4
Total	99.58 (0.1)	99.76 (0.4)			100.07

The numbers in brackets indicate the percent relative standard deviation of two replicate analysis.

The composition of fly ash from a single source is known to show variation with time. This is due to the differences in the mineralogical and chemical composition of different coal seams in the mine. The Sasol ash sample in this study is similar to that analysed the previous year by Campbell (1998), but with a lower CaO and SiO_2 content. The composition has however changed considerably since it was analysed in 1987 by Willis. The Arnot fly ash on the other hand shows very little variation since it was analysed by Willis in 1987.

4.1.2 Mineralogy

The mineralogical composition of fly ash is directly related to the mineralogy and chemical composition of the parent coal. The mineralogy of both Sasol and Arnot fly ash is typical of South African fly ash. The major mineralogical components of the ash are glass, quartz and mullite with accessory lime and hematite (Figures 4.1 and 4.2).

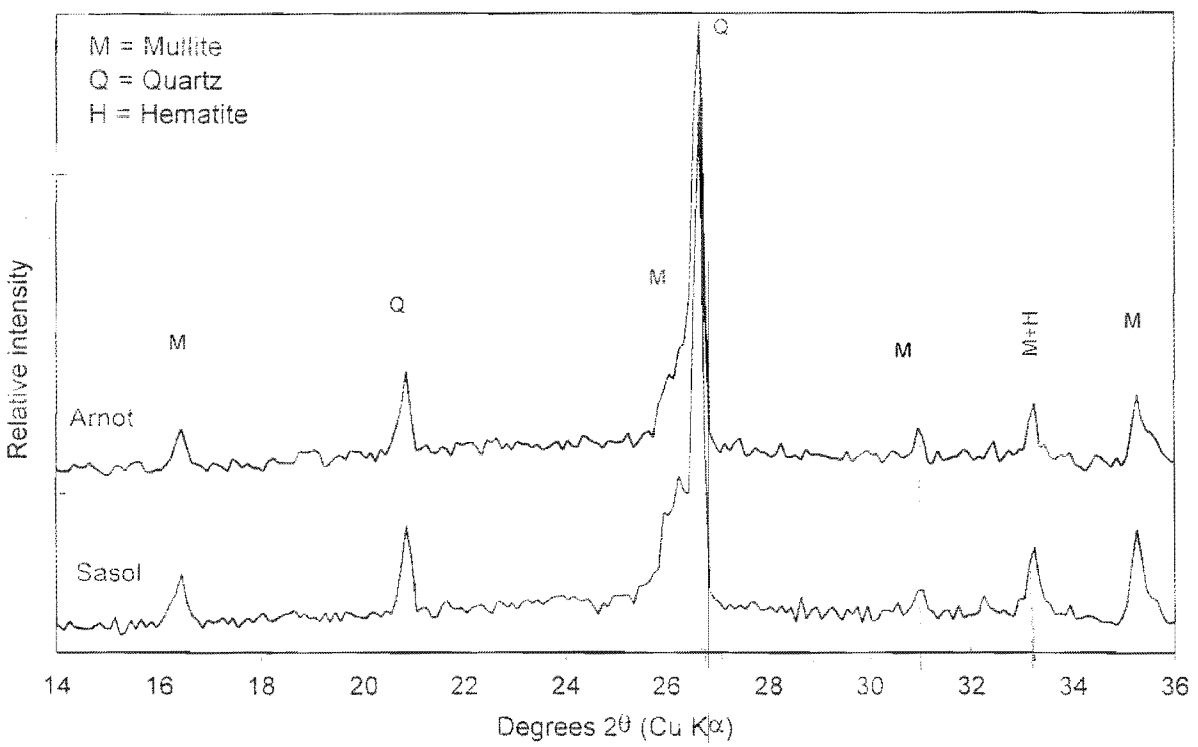

Figure 4.1: Diffractograms (14-36° 2θ) of fresh Arnot and Sasol fly ash obtained using Cu Kα radiation on pressed powder mounts

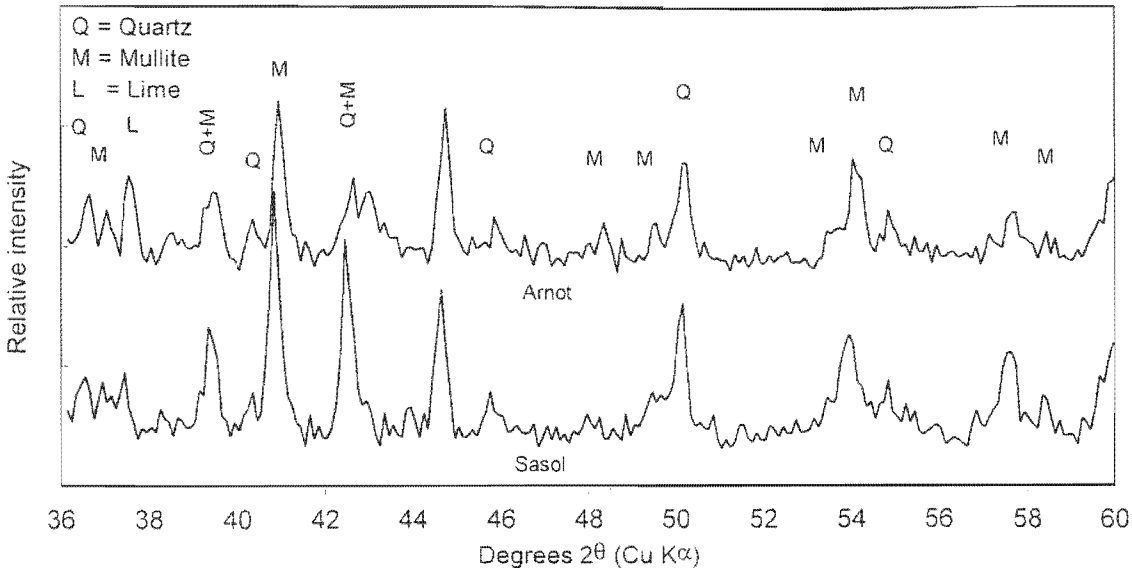

Figure 4.2: Diffractograms (36-70° 2θ) of fresh Arnot and Sasol fly ash obtained using Cu Kα radiation on pressed powder mounts

Although quantitative mineralogical analyses were not performed, a comparison of the peak areas can provide an indication of the relative abundance of the mineral phases present in the fly ash. The peak area is used rather than the peak height as it is considered to be more reproducible than the peak height for varying degrees of crystallinity and solid solution of a single phases (Bayliss, 1986, cited in Bosch, 1990). Using the peak area also compensates for the reduction in peak height and increased peak width of particles less than 0.1 μm in diameter (Alexander and Klug 1974, cited in Bosch, 1990).

The relative mineralogical compositions, based on the calculated peak areas of the quartz (100), mullite (110) and lime (000) peaks are given in Table 4.2. The selection of these peaks is based on the work of Bosch (1990) for quartz and mullite, although the angular range has been changed based on the peak profiles of the samples. The lime (000) peak has been used in this study as it has a higher intensity to the (111) peak used by Bosch (1990) which is barely detectable in the XRD pattern. The peak areas were calculated by integrating the area under curves using the trapezoidal rule after subtracting the average background of an adjacent angular range.

The relative proportion of hematite has not been determined as no clear peak is visible in either diffraction pattern. The presence of hematite in both samples is indicated by a small shoulder at 35.7 °2θ on the mullite peak at 35.3 °2θ.

There is no significant difference between the quartz content of the two fly ash samples, which suggests a similar quartz concentration in the parent coal. Quartz is the one major mineral present that is not affected by the higher temperatures of the furnace and survives the combustion process intact.

Table 4.2: Relative mineralogical composition of Arnot and Sasol fly ash based on peak area of x-ray diffraction analysis.

Phase	°2θ range	°2θ range background	Arnot	Sasol
Quartz (100)	20.45 - 21.05	19.35 - 20.35	33.5	34.7
Mullite (110)	16.05 - 17.05	14.95 - 15.95	18.5	28.0
Lime (000)	37.15 - 37.75	37.85 - 38.15	20.8	11.1
Glass	15.05 - 30.05	10.05 - 11.05	386.9	437.7

Research in the United Kingdom has shown the mullite content of fly ash to be dependent more on the mineralogical composition of the coal than the Al_2O_3 content (Willis, 1987). The mullite content is nevertheless well correlated with the Al_2O_3 concentration. The higher mullite content of the Sasol fly ash is supported by the higher Al_2O_3 concentration of this ash.

Diamond (1983) found that the position of the glass bulge maximum shifts towards higher 2θ values as the CaO concentration of the fly ash increases. The reason for this shift was speculated by Diamond (1983) to be due to the presence of a calcium aluminosilicate glass in high CaO fly ashes. Lesch (1987) found that the position of the X-ray diffraction maximum for the glass bulge shifted to higher 2θ values as the CaO concentration of the glass increased. No differences are observed with respect to the position of the glass bulge between the two samples (Figure 4.3).

The higher CaO concentration of the Arnot fly ash results in a higher lime concentration in the ash. The concentration of lime in the Arnot fly ash is twice that of the Sasol ash. Bosch (1990) found a strong correlation between the free lime and the CaO concentrations of South African fly ashes.

The infrared spectra (Figure 4.4) of the two fly ash samples are similar. The major absorption peaks observed correspond to Si-O-Si at 1060 cm^{-1} and Si-O-Si bending vibrations at 460 to 430cm^{-1}. The intensity of these absorption bands is much higher in the Sasol fly ash than the fly ash from Arnot. The differences in the intensity of the

absorption bands could be due to sample preparation procedures as KBr disks are do not replicate well. While the infrared absorption of the glass phase in the fly ashes may differ, the contribution of the Si-O-Si vibrations from both quartz and mullite to the spectra does not permit any conclusions to be made regarding differences in the glass compositon.

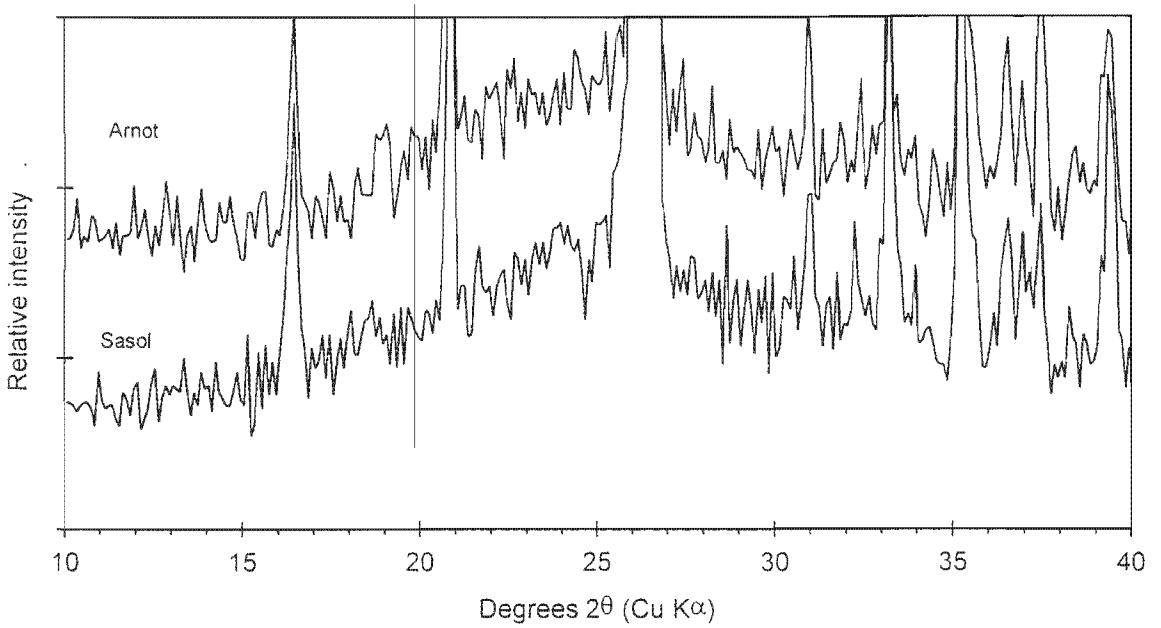

Figure 4.3: Diffractograms (10-40° 2θ) illustrating the size and position of the glass bulge of fresh Arnot and Sasol fly ash obtained using Cu Kα radiation on pressed powder mounts

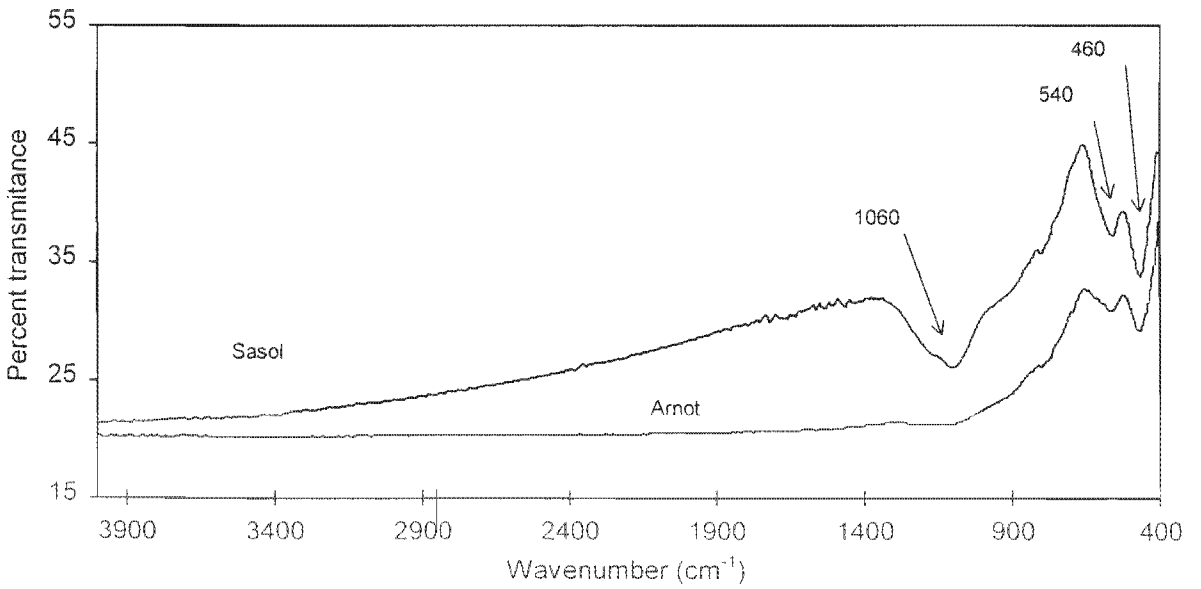

Figure 4.4: Infrared spectra of fresh Arnot and Sasol fly ash.

The SEM images of the two fly ashes are presented in Figures 4.5 and 4.6. The morphology of the Arnot fly ash is characterised by well rounded glass spheres. The higher proportion of glass spheres in the Arnot fly ash indicates a higher degree of melting of the mineralogical content of the parent coal. This can be attributed to a higher operating temperature in the furnace or to the higher CaO content of the mineral fraction. During burning CaO acts as a flux lowering the melting temperature of the mineral phases in the parent coal. A high CaO content in the parent coal results in a higher degree of melting and subsequently an increase in concentration of smooth glass spheres.

The Sasol fly ash on the other hand is characterised by an apparent larger grain size and more angular particles. These particles are similar to those described by (Hulett and Weinberger, 1980) as chunky mullite.

The results of the SEM EDXRF analyses of the fresh ash from Arnot and Sasol is presented in Table 4.3. Particles of both fly ashes are dusted with very fine specks. The analysis of these specks proved extremely problematic. Although no lime particles were identified in this study, Warren and Dudas (1984) found sub micron sized CaO fragments on the surface of the glass spheres. Sulphur was detected in the EDS spectra of of some coated particles, while no sulphur was detected in uncoeted particles. This indicates that some of the surface coatings are sulphate salts.

Table 4.3: SEM EDXRF data (peak intensities) of the EDS analysis of fresh fly ash from Arnot and Sasol presented in Figures 4.5b and 4.6b.

Analysis	Arnot_01	Arnot_04	Arnot_05	Sasol_1	Sasol_2	Sasol_6
Type	glass	glass	coated glass	glass	glass	mullite
Na	44					47
Mg	65	110	196	106	61	47
Al	3072	1848	145	3726	2034	3971
Si	3704	2316	187	4466	5100	3759
S			375			
K	44			79		47
Ca		248	1439	185	182	47
Ti	44			53	91	
Fe			145	26	30	

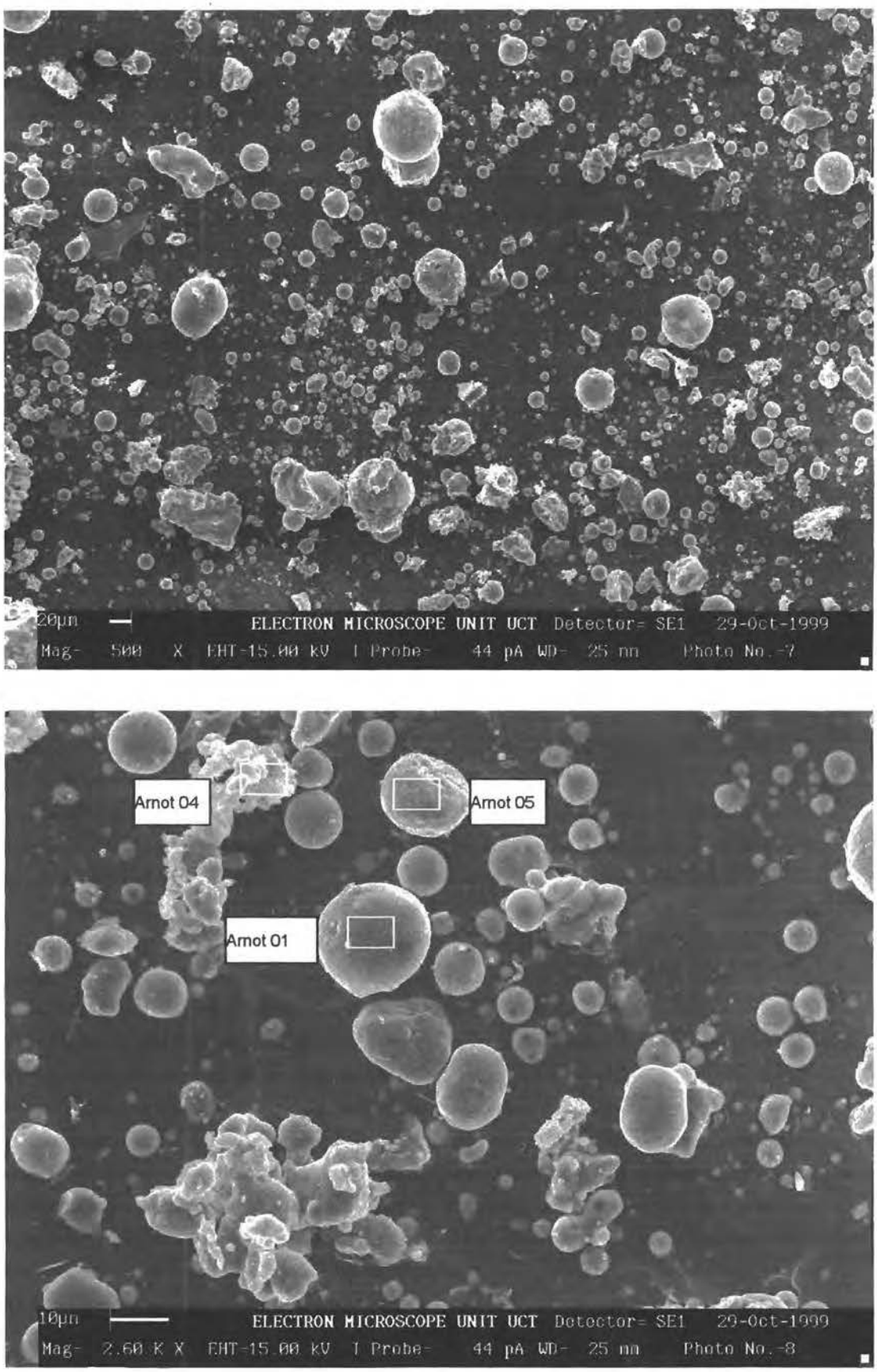

Figure 4.5: SEM image of fresh Arnot fly ash at a) low magnification 500x, and b) high magnification 2600x. These images illustrate the abundance of smooth rounded glass spheres.

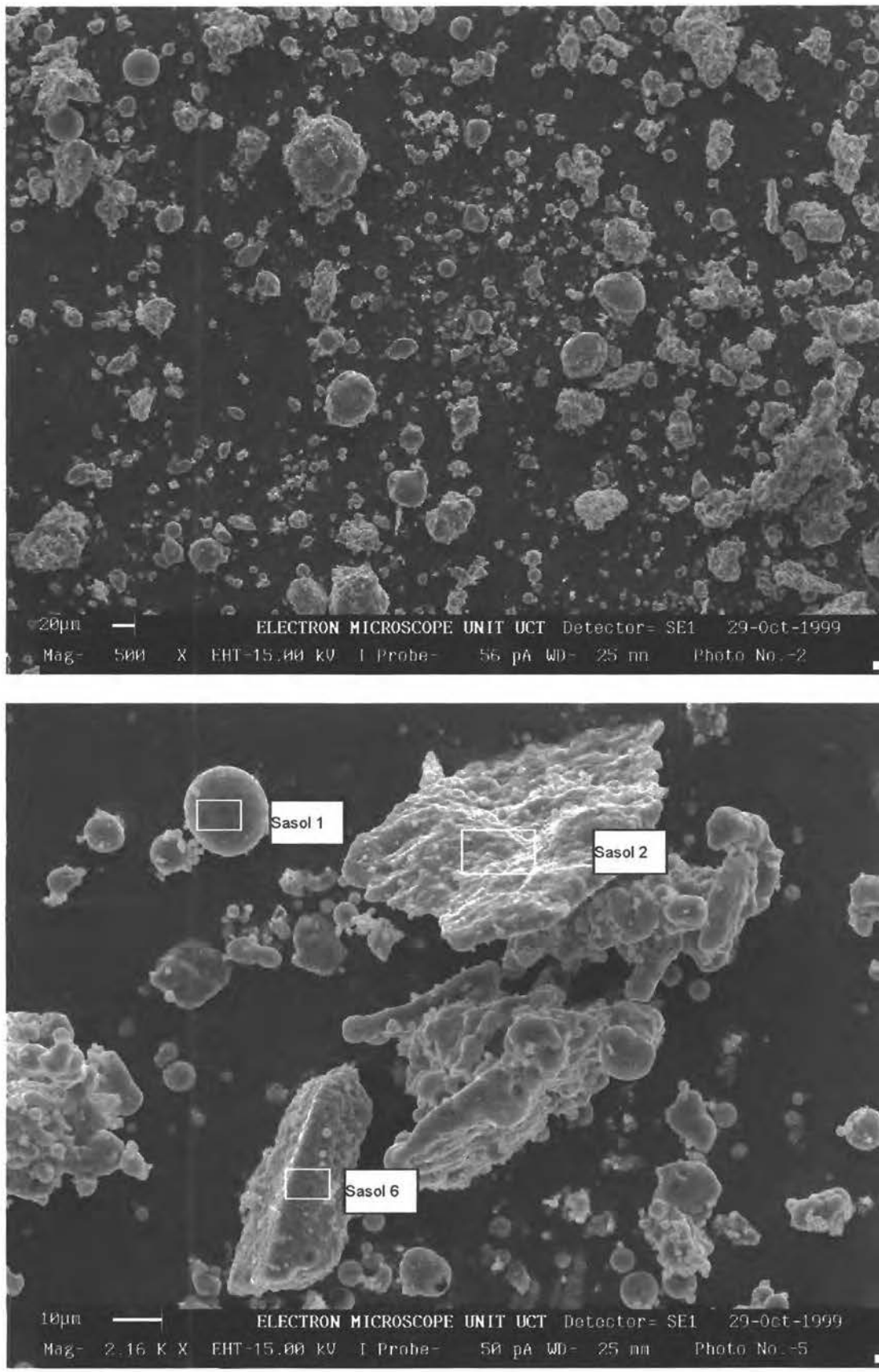

Figure 4.6: SEM image of fresh Sasol fly ash at a) low magnification 500x, and b) high magnification 2160x. These images reveal the sub rounded and blocky nature of the fly ash particles.

4.1.3 Saturated paste extracts

The chemical composition of the saturated paste extracts should reflect the composition of the more readily soluble salts of the fly ash. During cooling the inorganic species present in the vapour phases condense on the surface of the fly ash particles. The most common of these surface coatings is gypsum.

The chemical composition of the paste extracts are presented in Table 4.4. These solutions are both characterised by high pH and EC and high concentrations of Ca and SO_4^{2-}. The high pH of these solutions is most likely derived from the hydration and dissolution of lime. The dissolution of gypsum and other alkali sulphates are possibly responsible for the high SO_4^{2-} concentration. During the preparation of the Sasol fly ash extract a smell of NH_3 was evident which was confirmed by the analysis of the paste extract. No NH_3 was detected in the Arnot fly ash extract by smell or IC. The origin of the NH_3 in the Sasol fly ash is not known.

The higher concentration of CaO in the Arnot fly ash is not reflected in the paste extract. The Sasol fly ash extract has nearly double the SO_4^{2-} concentration of the Arnot fly ash extract, but the concentration of CaO in the fresh ash is nearly half that of the Arnot fly ash. The SO_4^{2-} concentrations of both extracts are however very similar. A possible explanation for the lower Ca concentrations in the Arnot extract could be due to the formation of ettringite. The saturation indices for selected minerals were calculated using the computer code PHREEQC (Parkhurst, 1995) are presented in Table 4.5. The solubility product of ettringite determined by Myneni *et al.* (1998a) of $10^{-111.6}$ was used for these calculations. These calculations indicate that the Arnot paste extract is supersaturated with respect to ettringite. No saturation indices for the Sasol ash extract could be calculated as no Al was detected in the solution. The saturation indices also indicate that these solutions are in equilibrium with both portlandite ($Ca(OH)_2$) and gypsum.

The presence of Al in the Arnot fly ash extract suggests the dissolution of the aluminosilicate glass, this should however be accompanied by an increase in the Si concentration. The concentration of Si is below the detection limit, which could indicate the precipitation of a silicate mineral such as wollastonite. The saturation index for wollastonite in the Arnot paste is calculated to be 0.9 assuming the Al concentration is equal to the detection limit. This calculation suggests a possible

explanation for the low Si concentration in the extract.

Table 4.4: Composition of saturated paste extracts

	Arnot	Sasol
pH	12.6	12.5
EC (mS/cm)	8.1	8.0
Na^+ (mg/L)	19	46
NH_4^+	<1.0	96
K+	<4.0	16
Mg*	1.7	1.3
Ca^{2+}	1414	2388
F^-	0	0
Cl^-	0	0
SO_4^{2-}	4752	4218
Al*	4.2	<1.0
Fe*	<1.0	<1.0
Si*	<1.0	<1.0

Table 4.5: Calculated saturation indices for saturated paste extracts.

	Arnot	Sasol
Ettringite	10.4	
Brucite	3.1	2.9
Gypsum	0.7	0.8
Portlandite	0.3	0.4
Lime	-9.8	-9.7

4.1.4 Discussion

The CaO concentration of a fly ash is expected to have a pronounced effect on its ability to neutralise acid mine drainage. A high CaO concentration in the coal lowers the melting temperature of the coal mineral fraction, resulting in a fly ash with a more Ca rich glass and higher concentration of lime. The lower melting temperature will result in a higher concentration of aluminosilicate glass in the fly ash. The higher melting temperatures associated with low CaO coal will on the other hand promote the formation of mullite.

The higher lime content of the Arnot fly ash is not reflected in the saturated paste extract. This could be due to the precipitation of ettringite and possibly wollastonite as indicated by the high saturation indices for these phases. The presence of Al in

the saturated paste extract of the Arnot fly ash indicates the dissolution of an Al rich phase, most likely the glass.

The importance of the higher mullite concentration in the Sasol fly ash is that it is less reactive than the glass phase and quartz (Wesche, 1991). The more reactive nature of the Arnot glass is indicated by the presence of Al in the saturated paste extract.

The Arnot fly ash is expected to show a greater neutralisation potential than the Sasol ash. While this neutralisation potential is expected to relate predominantly to the higher lime concentration, the contribution from dissolution of the glass may be important.

4.2 Batch neutralisation experiment

The titration curves for the Arnot and Sasol fly ashes are shown in Figure 4.8. The percentage ash in the mixtures has been calculated by weight assuming a density 1 g/cm^3 for the AMD. The two curves have the same basic shape indicating that the chemical reactions taking place in both systems are similar. The titration curves of both fly ash samples show three distinct regions of pH buffering. At ash percentages greater than 30% both fly ashes equilibrate at pH values of 12.7. The second buffering region occurs between pH values of 12.7 and 10.3. In this region the pH decreases slowly with the decreasing percentage ash. Below pH 10.3 very little buffering occurs and the pH decreases rapidly to values of about 4.5. The third buffering region is only observed in the Sasol fly ash, and occurs below a pH value of 4.5.

Figure 4.9 illustrates the change in the electrical conductivity during the neutralisation reactions. The EC shows an initial increase and then decreases with decreasing ash content, to a minimum at 16.6 % ash (ash: AMD = 1:5). As the percentage ash decreases further the EC rises again. These results show that the precipitates formed between pH 12.0 and 11.1 have the greatest ability to reduce the total dissolved salt load.

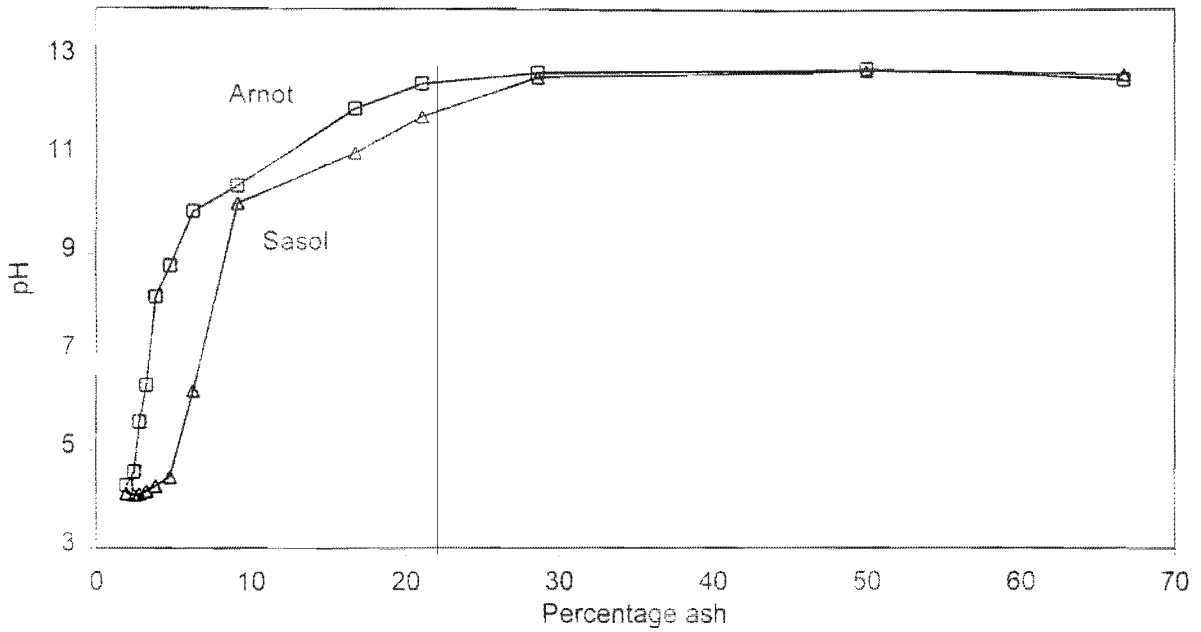

Figure 4.8: The titration curve for Arnot and Sasol fly ash with simulated AMD.

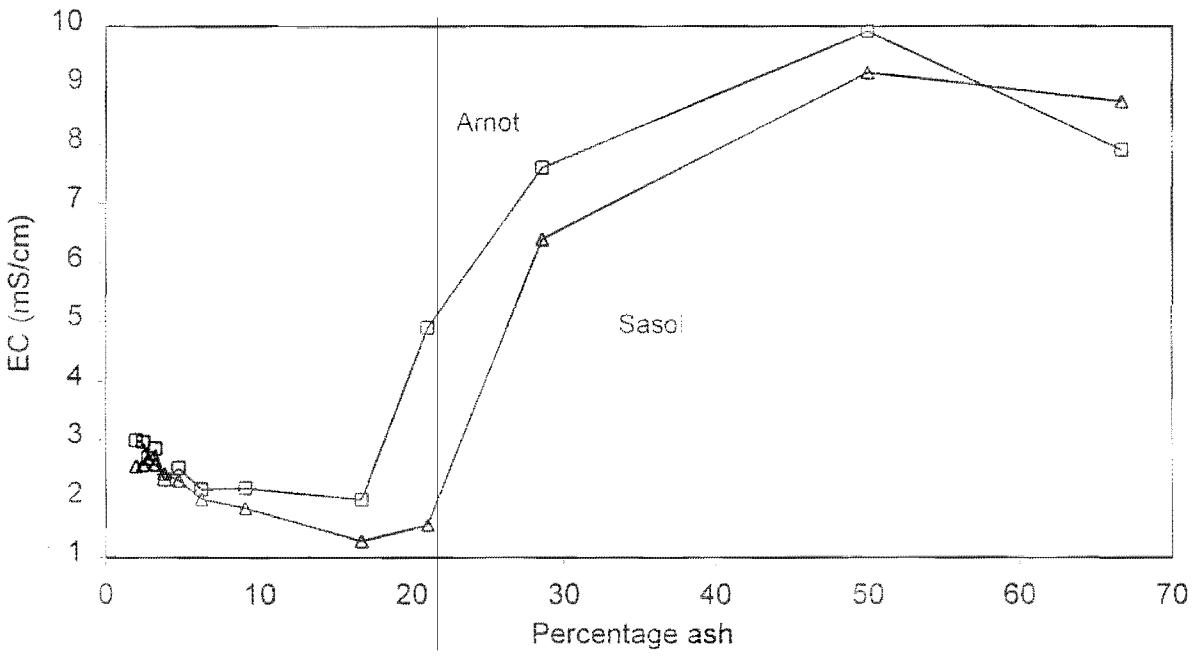

Figure 4.9: The variation of the electrical conductivity as a function of the percentage fly ash.

As the Arnot fly ash has a higher concentration of lime than the Sasol ash, the results are not directly comparable. The data in figure 4.8 has been normalised to the CaO concentration of the fresh fly ash and is depicted in Figure 4.10. The two curves overlay extremely well at pH values greater than 10. Below pH 10 the Sasol ash displays very little buffering capacity and the pH decreases very rapidly to a value of

4.5. The Arnot fly ash on the other hand shows a moderate buffering capacity in this pH region.

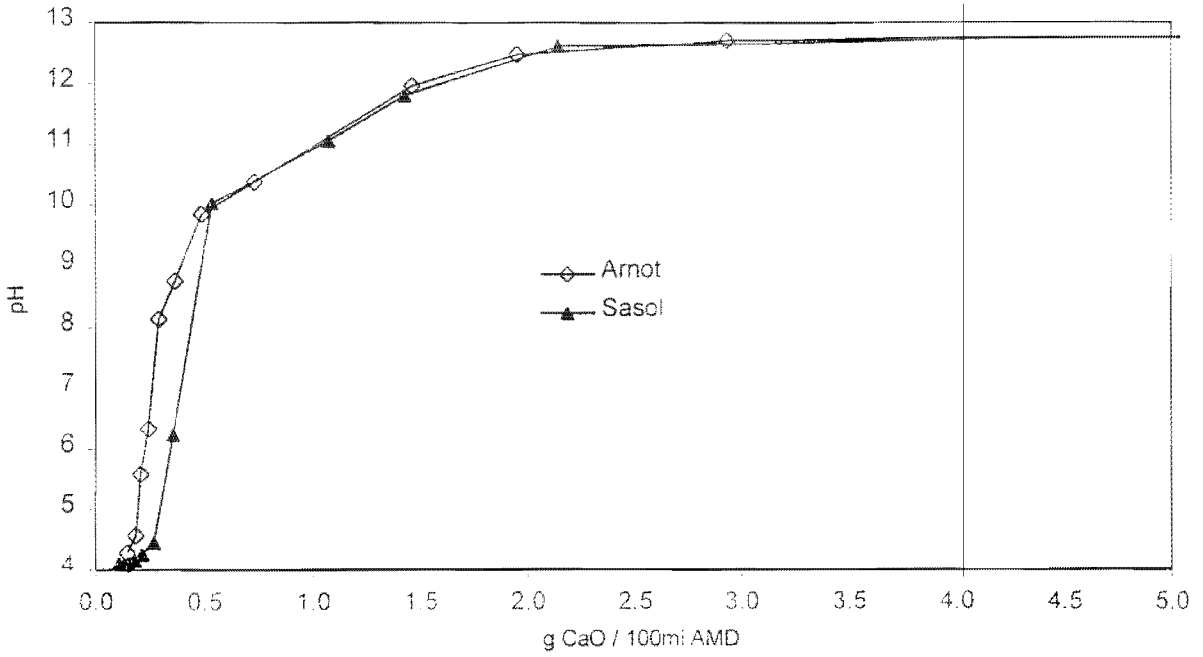

Figure 4.10: The change in solution pH for Arnot and Sasol ash expressed as a function of CaO concentration of the fresh fly ash. 5g CaO/100mL AMD corresponds to 50% Arnot fly ash and 30 % Sasol ash.

4.2.1 Precipitate mineralogy

The mineralogy of the precipitates was investigated by XRD using the <5μm fraction. The fine fraction was separated so as to reduce the background associated with the large amount of amorphous material in the bulk fly ash. No differences are found with respect to the minerals formed in both fly ash samples. In both fly ash samples the mineralogical phases identified were ettringite and gypsum. The results of the XRD analyses of the Arnot and Sasol fly ash are presented in figures 4.11 and 4.12, respectively. Only the peaks of ettringite and gypsum have been labelled, the remaining peaks originating from quartz and mullite (Figures 4.1 and 4.2).

Ettringite is a calcium aluminium sulphate hydrate that is common in highly alkaline sulphate environments. Bezuidenhout (1995) proposed the formation of ettringite as a possible reason for the observed decrease in sulphate concentration in an ash dam leachate. Campbell (1998) confirmed the presence of ettringite in fly ash, and associated its formation with the hardening of ash dams.

The crystal structure of ettringite can be considered as rows of $Al(OH)_6^{3-}$ octahedra bonded by three Ca^{2+} cations (Moore and Taylor 1970). Water molecules complete the co-ordination number of calcium. These columns consisting of $\{[Ca_6[Al(OH)_6]_2 \cdot 24H_2O]^{6+}\}$ are held together by sulphate which occur at four positions. The isomorphous substitution of the central Al^{3+} cations by other trivalent cations is also possible.

Ettringite is only stable in high pH environments. The congruent dissolution of ettringite can be described by the following equation (Myneni *et al.*, 1998a):

$$Ca_6Al_2(SO_4)_3(OH)_{12} \cdot 26H_2O \leftrightarrow 6Ca^{2+} + 2Al^{3+} + 3SO_4^{2-} + 12OH^- + 26H_2O \quad (4.1)$$

This reaction can also be written by substituting $Al(OH)_4^-$ for Al^{3+} in the products, which would be more correct, given the high pH at which ettringite is stable. Below pH values of 10.7 ettringite dissolution is incongruent, forming a mixture of gypsum and amorphous $Al(OH)_3$.

Ettringite is only present in samples that equilibrated above pH values of 10 and below pH values of 12. Below pH of 10 the only secondary mineral identified is gypsum, which persists to pH 5.6. Below pH 5.6 no secondary minerals are detectable by XRD. The observed relationship between ettringite and gypsum is in agreement with the incongruent dissolution of ettringite below pH values of 10.7 to gypsum and amorphous $Al(OH)_3$. As amorphous $Al(OH)_3$ is not detectable by XRD the fate of the Al in the AMD can only be inferred from the thermodynamic modelling of the solution chemistry.

No iron phases were detected by XRD in any of the reaction products. As the concentration of iron in solution was below the detection limit for all solutions above pH values of 5, some secondary iron phases must be present. The reasons for the lack of any iron phases in the precipitates could be that the concentrations are below the detection limit of XRD. This reason would be more relevant at the high pH values where the amount of iron added to the ash is small. Another possible explanation is that the iron precipitates have formed coatings on the fly ash particles, which have not been dislodged by the ultrasonic probe. Iron oxides commonly form coatings on quartz particles (Drever, 1997), and this is thought to be a far more likely explanation.

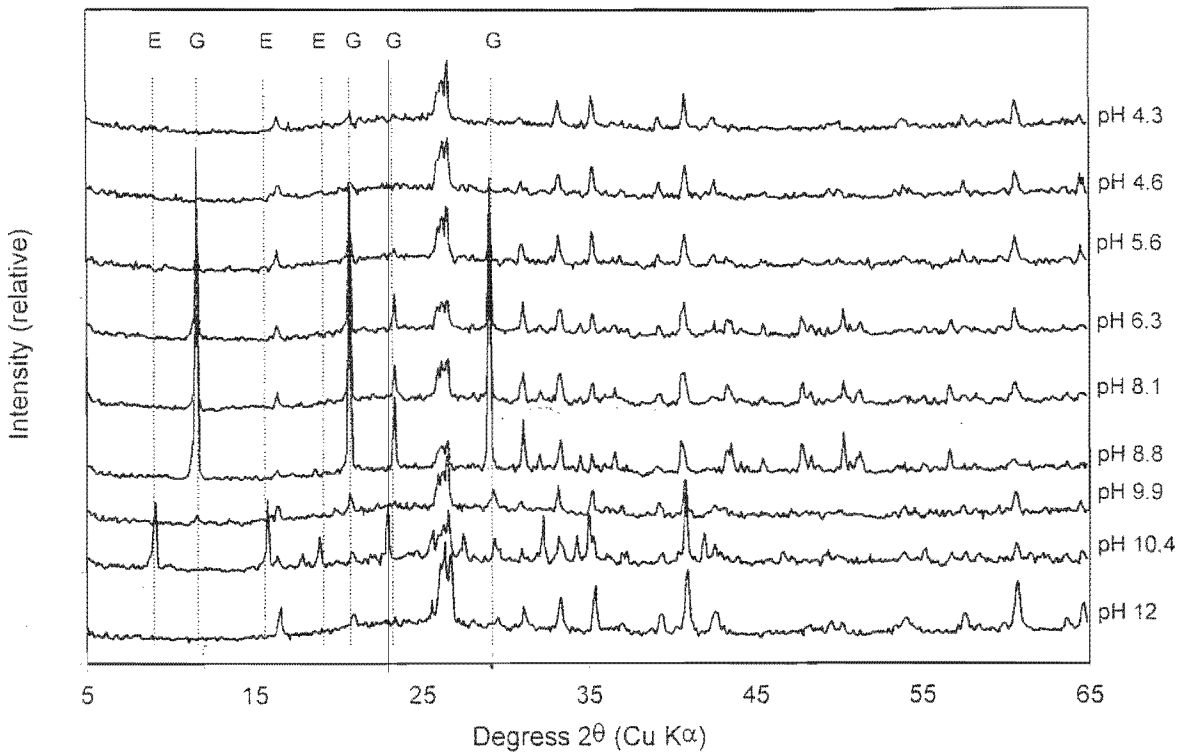

Figure 4.11: X-ray diffraction patterns of the <5μm fraction of Arnot fly ash after reacting with AMD. Ettringite (E) and gypsum (G).

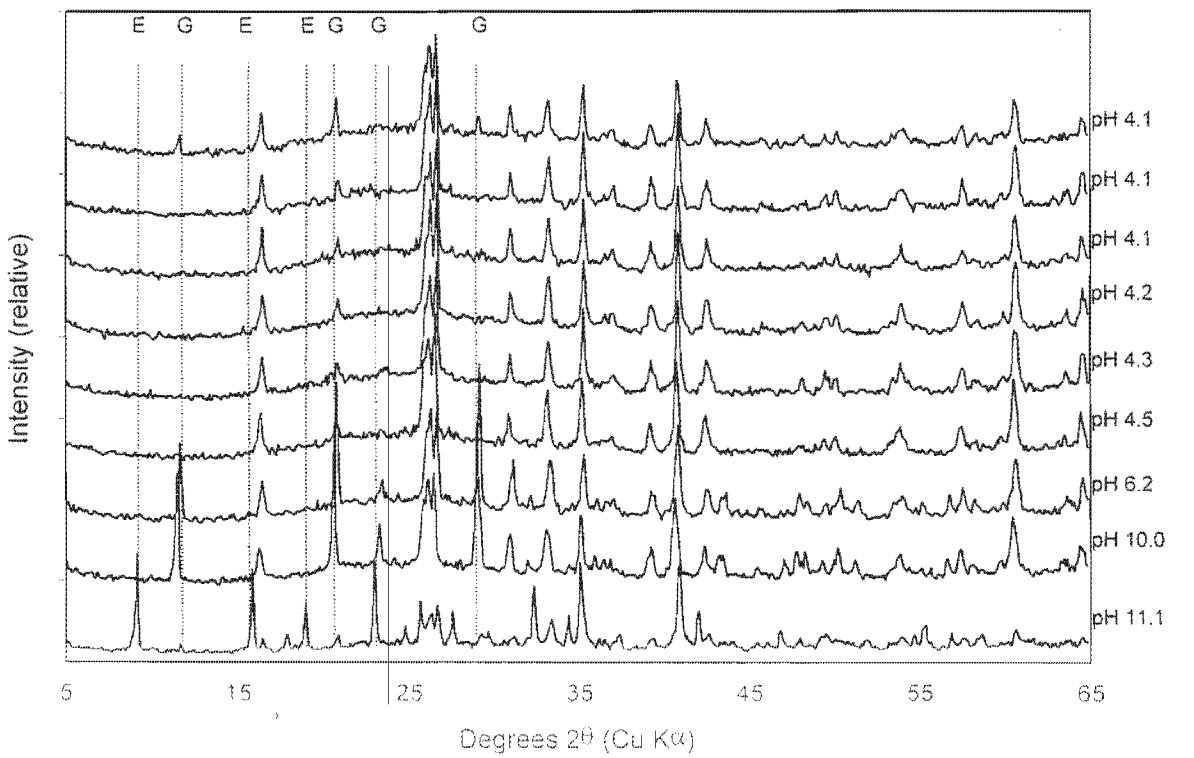

Figure 4.12: X-ray diffraction patterns of the <5μm fraction of Sasol fly ash after reacting with AMD. Ettringite (E) and gypsum (G).

Scanning electron microscopy was employed as an aid in the identification of the secondary precipitates. Due to time constraints not all of samples could be investigated. Three samples of each ash were selected for SEM analysis. The selection was based on the results of the XRD analysis to include samples which equilibrated at high, low and neutral pH values. The samples selected to represent the Arnot fly ash were A1/5, A1/35 and 1/50, which equilibrated at pH values of 10.4, 5.6 and 4.3, respectively. Samples S1/5, S1/15 and S1/50 were selected from the Sasol fly ash and equilibrated at pH values of 11.1, 6.2 and 4.1, respectively.

The errors involved with SEM EDXRFS analysis of micron sized particles can be large. The analysing volume in a SEM EDXRF system is in the order of $2\mu m^3$. The size of secondary precipitates observed in the samples is generally about $2\mu m$ in width. As the analysing volume is frequently larger than the crystal, the analysis includes an unknown contribution from the surrounding matrix. This contribution from the matrix can be corrected for, provided that one of the elements analysed is present in one phase only. This contribution from the surrounding matrix makes the differentiation between ettringite and gypsum extremely difficult, as the high aluminium signal from the fly ash particles is present in all analyses of small crystals.

The SEM images from the Arnot fly ash are presented in Figures 4.13 and 4.14 and those from Sasol in Figures 4.15 and 4.16. The results of the SEM EDXRF analysis are presented in Table 4.6. The peak intensities are expressed as a percentage of the total counts to account for differences in the counting times.

Ettringite could not identified with any degree of certainty in the high pH sample from Arnot, but could be in the Sasol sample. Figure 4.13 illustrates a mass of fine needle shaped crystals that have precipitated on an irregularly shaped fly ash particle. The EDS spectrum for this precipitate (Arnot2_02) shows an increase in the intensity of the sulphur peak relative to the uncoated spheres of the fresh ash indicating a sulphate phase. The pH of the sample indicates that ettringite is the stable sulphate phase, but the precipitation of gypsum during the drying of the sample cannot be ruled out. Figure 4.15 shows a relatively large ettringite crystal formed in the Sasol ash at pH 11.1. The SEM EDXRF analysis of this crystal (Sas15/3) showed a small contribution from the surrounding fly ash. The Al/Si ratio is 2 compared with a ratio of

close to 1 for the glass. This indicates the presence of Al in the crystal and supports the identification of this crystal as ettringite.

Figures 4.14 and 4.16 show two coated fly ash particles from Arnot and Sasol, respectively. The results of the EDS analyses show that the coating consists of iron. The precipitate coating the particle in Figure 4.16 consists of sub micron sized spherical particles that have aggregated on the surface of the fly ash particle. This morphology is typical of ferrihydrite and particularly 2-line ferrihydrite (Cornell and Schwertmann, 1996).

Table 4.6: Results (peak height) of the SEM-EDS analysis of secondary precipitates in Arnot and Sasol fly ash.

Analysis	Arnot2_02	Arnot2_06	Sas15/3	Sas2-2
O	835	992	618	36
Mg	74	48		
Al	1367	61	146	51
Si	1350		73	51
S	442		556	
Ca	974		413	
Fe	74	1155	18	1232

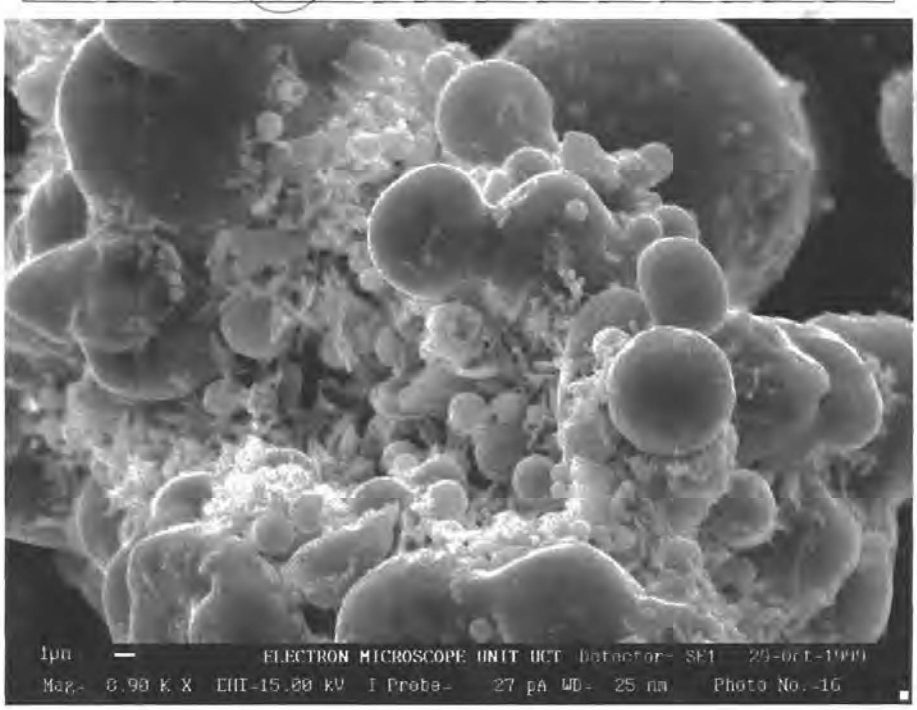

Figure 4.13: SEM image of ettringite needles filling hollows on an irregularly shaped fly ash particle from Arnot. At pH 10.4

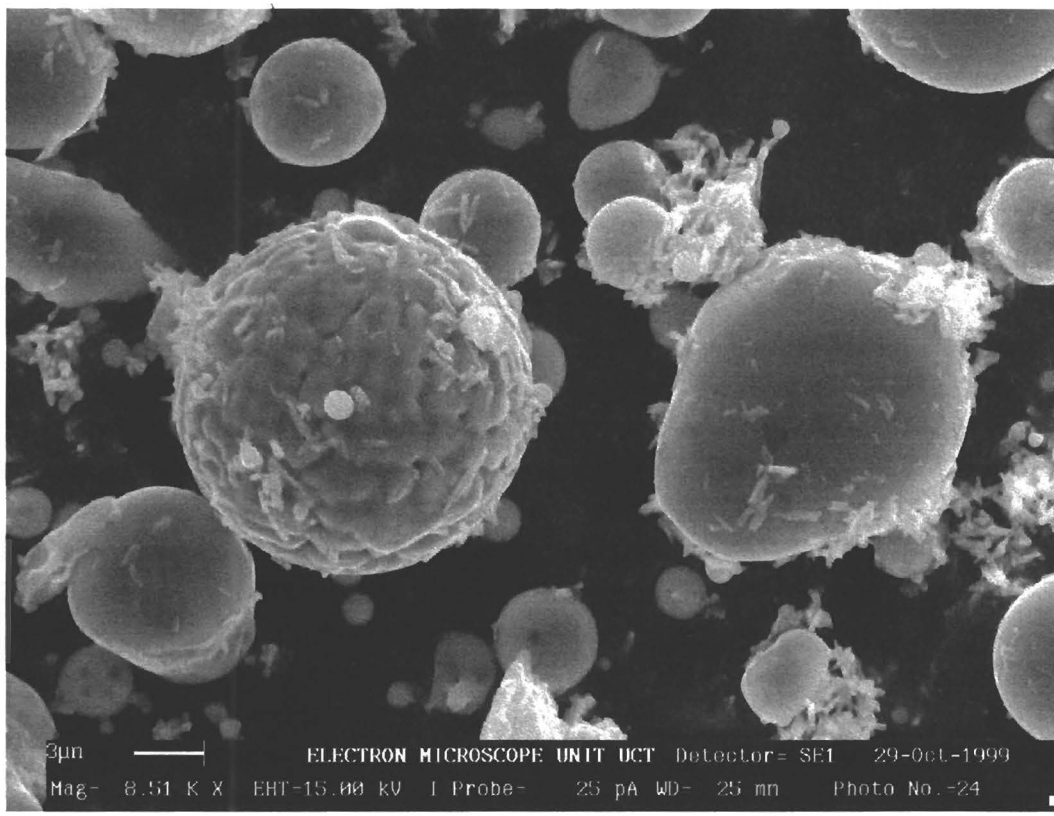

Figure 4.14: SEM image of an iron oxide coating on a glass sphere from Arnot.

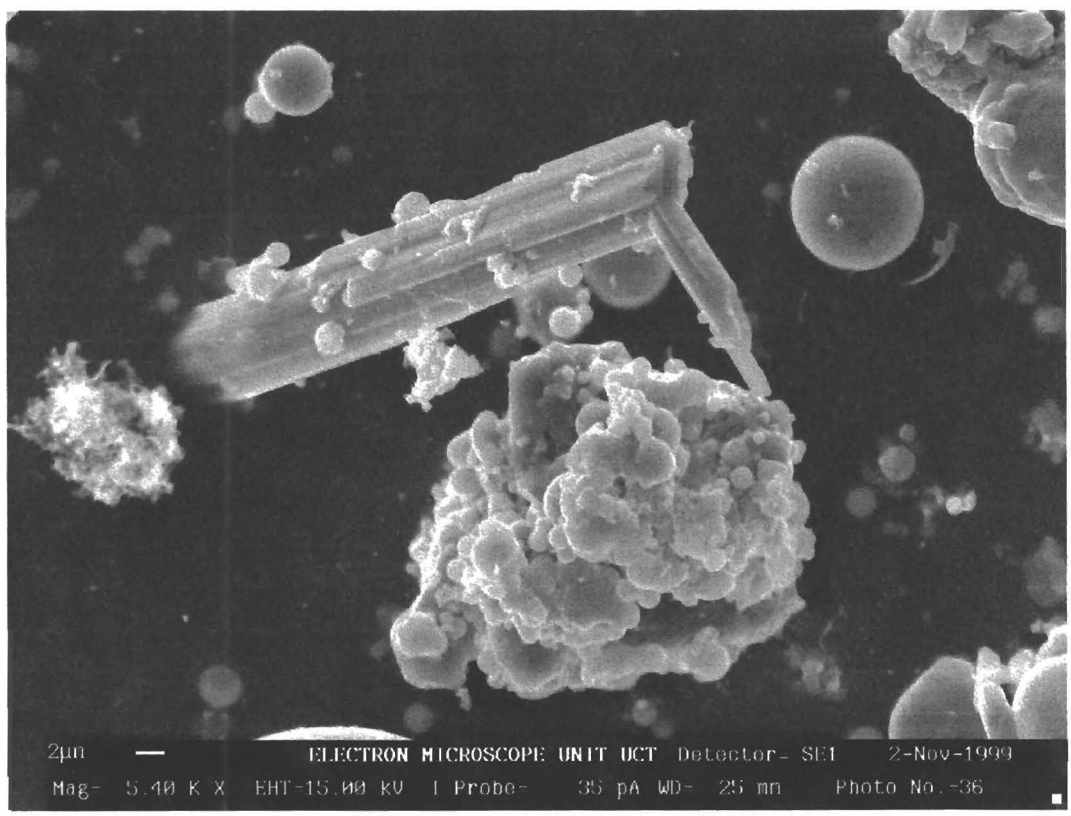

Figure 4.15: A large ettringite crystal precipitated in the Sasol fly ash at pH 11.1

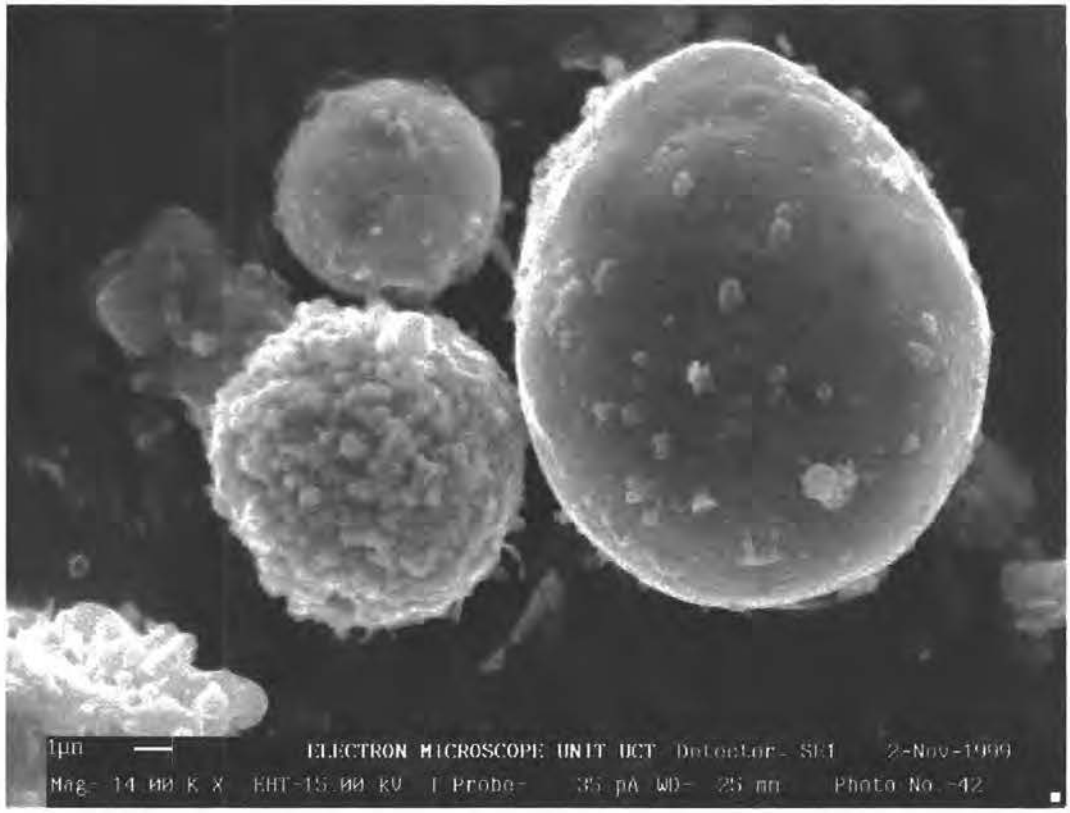

Figure 4.16: A 1µm glass sphere coated with ferrihydrite in the Sasol fly ash at pH 4.1.

To gain a better understanding of the precipitate mineralogy, particularly iron, saturated paste extracts of both fly ash samples were titrated with AMD to pH 4, 5, 6, 7, 8, 9, 10, 11 and 12. The precipitates were characterised by FTIR and selected samples by XRD. The results of the FTIR analysis are presented in Figures 4.17 and 4.18. While the FTIR spectra have not been used to identify the mineralogy of the precipitates, they do allow the precipitates to be grouped.

The precipitate mineralogy was classified into three groups based on the FTIR spectra. The spectra of the precipitates at pH 12, 11, and 10 have a characteristic absorbance band in the region of 890 cm^{-1}. The precipitates formed at pH 6, 5 and 4 do not have any absorption band between 1300 and 1550 cm^{-1}. The precipitates formed at pH 9, 8 and 7 have been grouped together as they do not have an absorption band at 890 cm^{-1} but do show two absorption bands between 1300 and 1550 cm^{-1}.

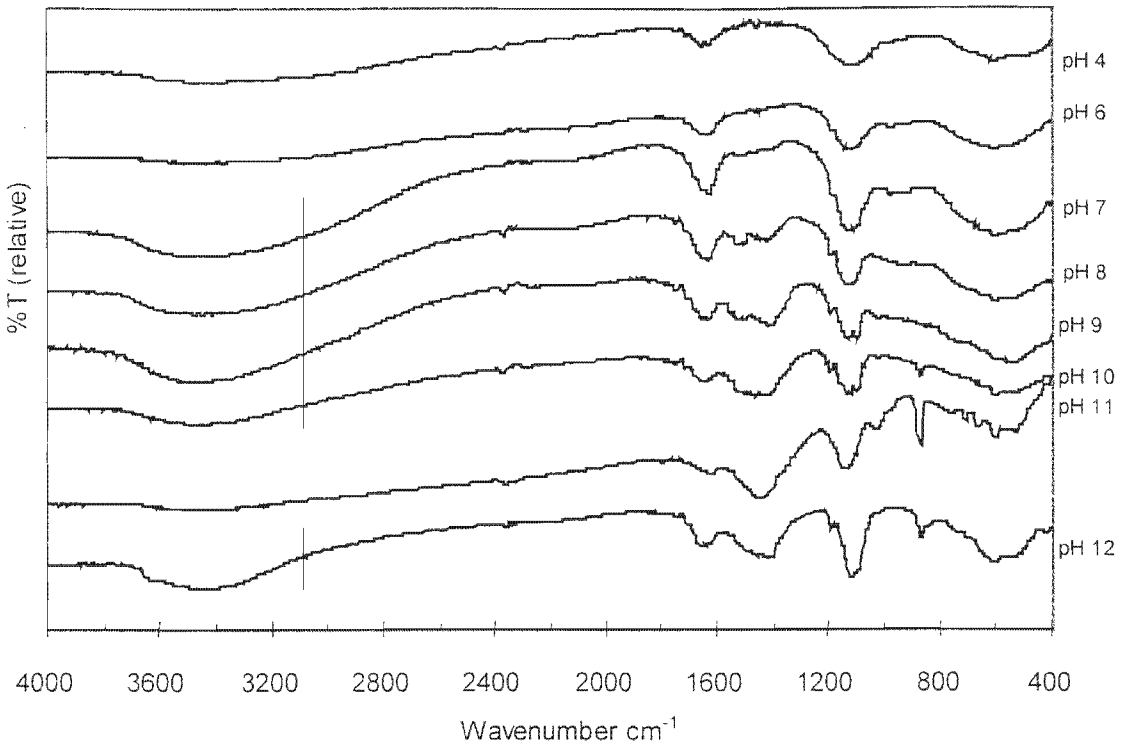

Figure 4.17: FTIR spectra of precipitates formed from Sasol paste extracts and AMD.

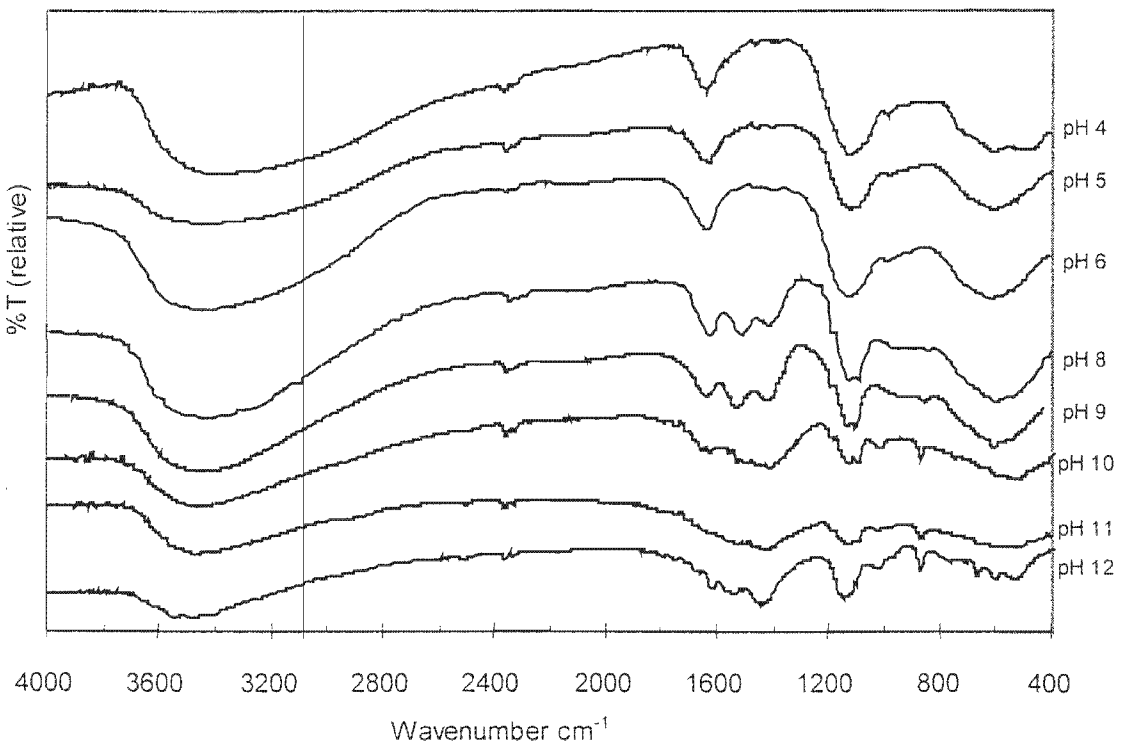

Figure 4.18: FTIR spectra of precipitates formed from Arnot paste extracts and AMD.

The precipitates at pH values of 11, 8 and 5 were selected as being representative of the three groups. To obtain sufficient precipitate for XRD analysis, 50mL of saturated paste extract was titrated with AMD.

The diffraction patterns of these precipitates is presented in Figure 4.19. At pH values of 5 and 8 the precipitate formed was identified as 2-line ferrihydrite and no other phases were identified. The precipitate formed at pH 11 was identified as ettringite. No ferrihydrite could be identified. The precipitate does, however, have a reddish colour indicating the presence of iron oxides, and the amount of ferrihydrite formed at pH 11 is probably well below the detection limit.

Although hematite and goethite are the most thermodynamically stable ferric oxide minerals under aerobic surface conditions, ferrihydrite may be kinetically favoured due to the Ostwald step rule (Schwertmann and Fitzpatrick, 1992). Ferrihydrite commonly forms as a result of the rapid oxidation and hydrolysis of Fe^{2+} (Schwertmann and Fitzpatrick, 1992; Bigham *et al.*, 1992). Ferrihydrite typically occurs as highly aggregated spherical particles, 2-6 nm in diameter (Bigham *et al.*, 1992). Ferrihydrite is poorly crystalline and displays weak XRD patterns varying from 2 line to 6 line profiles. The small particle size of ferrihydrite results in a high surface area and a significant adsorption capacity for other metals in solution and anions. The anion adsorption capacity decreases with increasing pH.

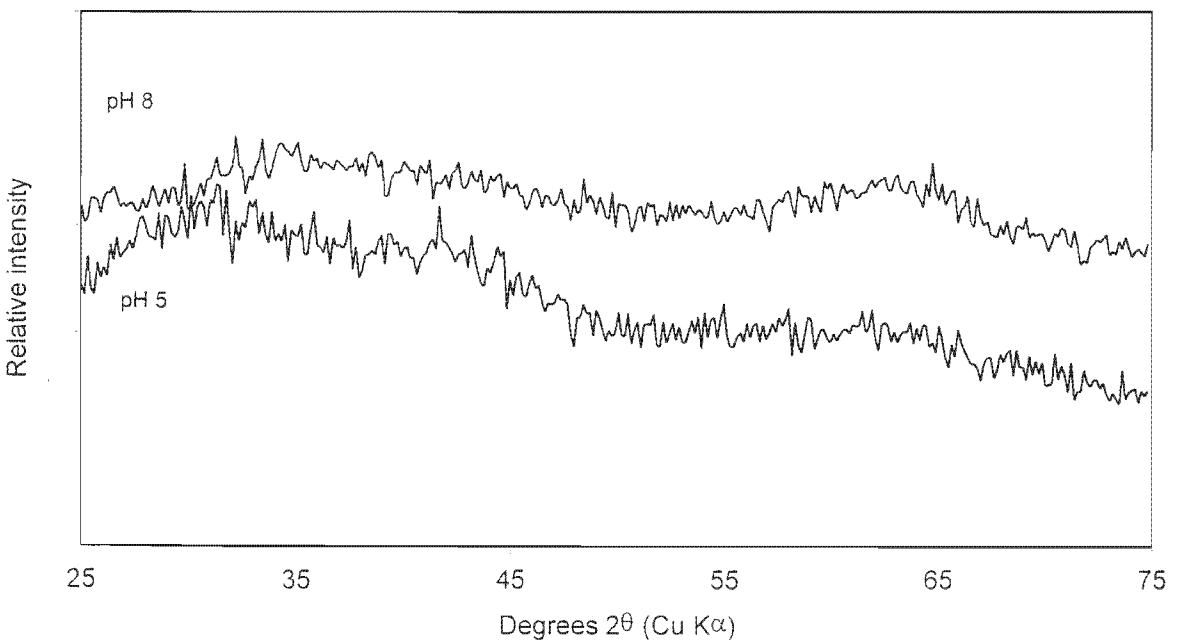

Figure 4.19: XRD patterns for ferrihydrite precipitated at pH 5 and 8.

4.2.2 Solution chemistry

The thermodynamic modelling of the solution chemistry was performed using the

program PHREEQC (Parkhurst, 1995) version 1.6, utilising the MINTEQA2 (Allison *et al.*, 1991) thermodynamic database. No changes were made to existing thermodynamic data in the database, although the lack of any data for ettringite required this phase to be added.

In selecting the solubility product for ettringite two values were found in the literature. Myneni and co workers (1998) and Atkins *et al.* (1991) reported a value of $10^{-111.6}$ and $10^{-111.3}$, respectively for the reaction:

$$Ca_6Al_2(SO_4)_3(OH)_{12}\cdot 26H_2O \leftrightarrow 6Ca^{2+} + 2Al^{3+} + 3SO_4^{2-} + 12OH^- + 26H_2O$$

Reardon (1991) determined the solubility product of ettringite to be $10^{-43.13}$ for the reaction:

$$Ca_6Al_2(SO_4)_3(OH)_{12}\cdot 26H_2O \leftrightarrow 6Ca^{2+} + 2Al(OH)_4^- + 3SO_4^{2-} + 4OH^- + 26H_2O \quad (4.2)$$

These two solubility products are related to each other by the aluminium hydrolysis constants for the reaction products, and yield very similar results. Although the two solubility products are similar the value calculated by Myneni and co workers (1998a) has been used, as the experimental procedures used involved equilibration from both the undersaturated and supersaturated state.

The chemical composition of the Arnot and Sasol fly ash AMD filtrates are presented in Tables 4.7 and 4.8, respectively. The saturation indices for selected phases are presented graphically in figures 4.13 and 4.14.

The results of the modelling of the Arnot fly ash – AMD system shows that ettringite and wollastonite are the stable mineral phases above pH 10. The saturation indices for ettringite increase rapidly from low pH to a pH of 9.8 where the slope of the curve flattens before increasing slowly above pH 10.3. Above pH 10.3 the saturation indices for gypsum and amorphous $Al(OH)_3$ decrease while that of ettringite increases. This is in agreement with the proposed incongruent dissolution of ettringite below pH 10.7 to gypsum and $Al(OH)_{3(a)}$ (Myneni *et al.*, 1998a). There is a similar relationship between the saturation indices of quartz and wollastonite.

Table 4.7: The solution chemistry of the Arnot fly ash AMD filtrates.

Sample	A1/5	A1/10	A1/15	A1/20	A1/25	A1/30	A1/35	A1/40	A1/50
% Ash	16.7	9.1	6.3	4.8	3.8	3.2	2.8	2.4	2.0
pH	11.9	10.4	9.9	8.8	8.1	6.3	5.6	4.6	4.3
EC mS/cm	1.98	2.18	2.16	2.52	2.32	2.85	2.69	2.96	2.99
Na^+ mg/L	5.5	4.5	6.0	4.0	5.5	3.5	3.0	2.0	2.5
NH_4^+	1.0	2.0	4.5	1.5	1.0	0.5	1.0	2.0	4.0
K^+	3.5	2.5	3.5	3.5	2.0	1.0	1.0	0.5	2.0
Mg^{+2}	0.5	2.0	2.0	75.5	163	169	153	134	108
Ca^{+2}	577	865	841	822	637	672	727	769	676
Cl^-	91.5	94.3	83.6	90.65	89.95	87.1	88.3	90.5	92.8
SO_4^{-2}	14.6	1259	1186	1642	1993	2110	2422	2748	3330
Al	1.34	0.55	3.04	1.34	1.02			29.6	105
Si	4.42	2.65	2.25		1.04	2.84	4.48	15	13.9
Fe^{+2}							68.5	100	117
Fe^{+3}							12.0	14.1	9.5
Fe total							80.6	114	127

Table 4.8: The solution chemistry of the Sasol fly ash AMD filtrates.

	S1/5	S1/10	S1/15	S1/20	S1/25	S1/30	S1/35	S1/40	S1/50
% Ash	16.7	9.1	6.3	4.8	3.8	3.2	2.8	2.4	2.0
pH	11.1	10.0	6.2	4.5	4.3	4.2	4.1	4.1	4.1
EC mS/cm	1.29	1.84	1.99	2.31	2.42	2.59	2.68	2.57	2.55
Na^+ mg/L	10.0	8.6	6.5	5.0	4.0	5.5	4.0	3.0	5.5
NH_4^+	13.6	6.0	10.0	4.0	3.5	4.0	2.5	1.5	3.0
K^+	3.2	26.4	5.0	2.0	1.0	1.0	1.0	1.0	1.0
Mg^{+2}	1.2	2.8	48.0	38.0	32.5	25.0	25.0	20.5	17.0
Ca^{+2}	504	510	916	779	743	675	639	552	476
Cl^-	104	101	92.4	90.0	95.3	94.2	82.2	96.9	86.4
SO_4^{-2}	761	1534	1599	2261	3568	3605	3059	4017	3759
Al	0.2	16.4	0.8	39.9	120	172	196	247	295
Si	13.3	1.1	3.1	8.4	8.2	9.8	10.4	12.4	12.8
Fe^{+2}				124	138	154	161	165	185
Fe^{+3}				13.6	14.6	18.6	13.6	19.1	15.1
Fe total				138	152	173	174	184	200

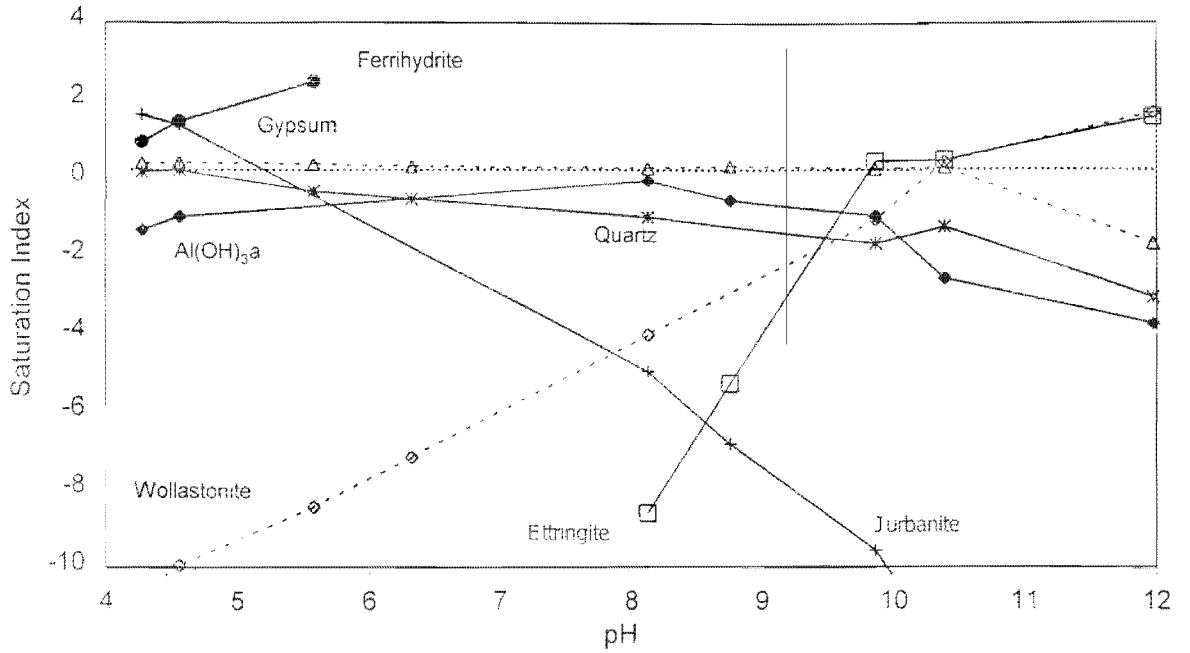

Figure 4.20: Saturation indices for Arnot fly ash – AMD extracts as a function of solution pH.

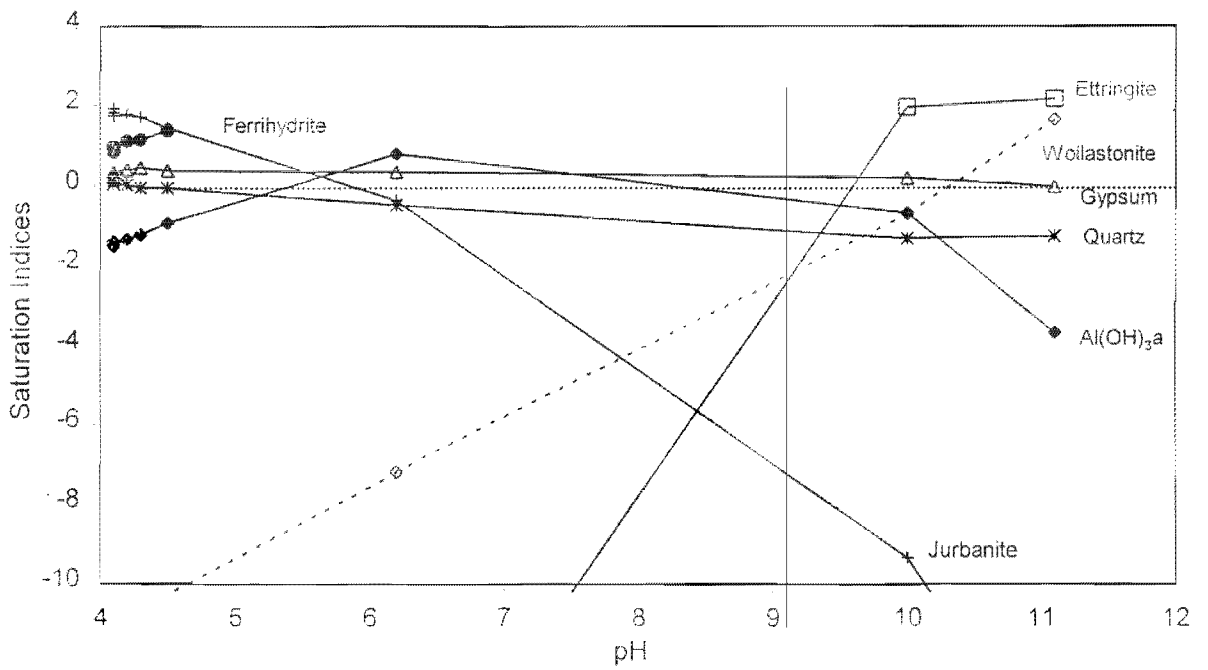

Figure 4.21: Saturation indices for Sasol fly ash – AMD extracts as a function of solution pH.

In the case of the Sasol fly ash the relationships between these phases is not as clear. Ettringite, wollastonite and gypsum are indicated as being stable minerals above pH 10. The saturation index of gypsum does not decrease as the pH increases above 10. The saturation index of $Al(OH)_{3(a)}$ does, however, follow the

predicted trend. The reason for this deviation is not clear, but could be related to the degree of supersaturation of the solution with respect to ettringite.

Between pH values of 5 and 10 the composition of the solutions of the two fly ashes suggest equilibrium with gypsum and near equilibrium with amorphous $Al(OH)_3$. Although the lack of analytical data on the Al concentration in this pH range hampers the modelling the Al geochemistry, amorphous $Al(OH)_3$ appears to be controlling the concentration of Al in solution.

Below pH 4.5 the solutions are in equilibrium with quartz. The lack of appropriate thermodynamic data for the calcium aluminosilicate glass does not allow the modelling of the glass phase. This indicates that the kinetics of quartz dissolution is quite rapid below pH 4.5 and equilibrium within 72 hours has been achieved. The saturation indices for amorphous $Al(OH)_3$ decrease rapidly below pH values of 4.5, together with an increase in the concentration of Al in solution. The dissolution of amorphous $Al(OH)_3$ below pH 4.5 is accompanied by an increase in the saturation index for jurbanite ($Al(SO_4)(OH).5H_2O$).

The saturation indices indicate that all solutions where iron was detected are supersaturated with respect to ferrihydrite. The high concentration of both ferric and ferrous iron in the solutions above pH 4 is unexpected. The factors that determine which oxide will form include pH, oxidation rate, temperature and foreign compounds within the system. The conditions which favour the formation of ferrihydrite include a pH <5, the presence of Si and a fast oxidation rate (Cornell and Schwertmann, 1996). The first two conditions are satisfied, but the oxidation rate might not be: after 72 hours between 30 and 60% of the iron is still in the ferrous state.

4.2.3 Discussion

The Arnot fly ash with its higher concentration of lime has a larger neutralisation potential per unit mass than the Sasol fly ash. The neutralisation potential of these two fly ashes is, however, very similar above pH 10 when expressed as a function of the CaO concentration of the fresh ash. Below a pH of 10 the Arnot fly ash shows a small but significantly larger ability to buffer the pH. This weak pH buffer is considered to be the result of the dissolution of the glass phase. The dissolution of the glass phase is supported by the presence of Si in the solutions.

The EC of the solutions for both fly ash samples show a minimum at 16.6% ash and coincides with the precipitation of ettringite. The EC achieved by the Sasol fly ash is lower than that reached by the Arnot fly ash. The concentration of SO_4^{2-} in the Arnot solution (14.6 mg/l) is however substantially less than that in the solution from Sasol (761 mg/l). The total dissolved solids (TDS) of the Arnot solution 698 mg/l compared to 1410 mg/l in the Sasol solution. The higher EC in the Arnot solution is attributed to the disproportionately large contribution of the OH^- anion to the EC at such a high pH value. Below pH 10 the EC increases steadily, this increase is attributed to the dissolution of ettringite and precipitation of gypsum and amorphous $Al(OH)_3$.

Between pH values of 12 and 10 the precipitate mineralogy consists of ettringite and 2-line ferrihydrite. The precipitation of ettringite could have significant implications with respect to the removal of trace contaminants from both the fly ash leachate and AMD. Myneni and co workers (1997) found that arsenate is complexed strongly with ettringite surface sites. The precipitation of ettringite can also result in attenuation of oxyanions by coprecipitation (Myneni *et al.*, 1998b).

Below pH 4.5 the mineral assemblage quartz, gypsum, ferrihydrite and jurbanite appears to control the solution composition. At intermediate pH values, between pH 10 and 5, geochemical modelling indicates that the solution composition is controlled by gypsum and $Al(OH)_{3(a)}$. X-ray diffraction analysis confirmed the presence of ferrihydrite in this pH range.

4.3 Kinetic studies

As the experiments were conducted at the ambient temperature, the EC measurements are highly variable in the time range 1 to 24 hours. As mentioned previously (section 3.3.1), the results of the experiment in this time frame were not reproducible. It is thought that this variability in the EC measurements might be the result of temperature fluctuations influencing the reaction rates in solution.

4.3.1 Arnot fly ash

The results of the kinetic experiments using Arnot fly ash: AMD ratios of 1:5, 1:10 and 1:20 are depicted graphically in Figures 4.22, 4.23 and 4.24.

At a ratio of ash: AMD of 1:5 the pH changes very rapidly reaching pH 10 within 30 minutes. The pH continues to increase but at a slower rate before reaching a maximum at pH 12.3 after 8 hours. The pH decreases slightly with time reaching a value of 11.9 after 72 hours. The EC shows a rapid increase to 4.2 mS/cm after 1 hour, after which the general trend is for the EC to decrease. By the time the experiment was ended at 72 hours the EC was 1.9 mS/cm and had not yet stabilised.

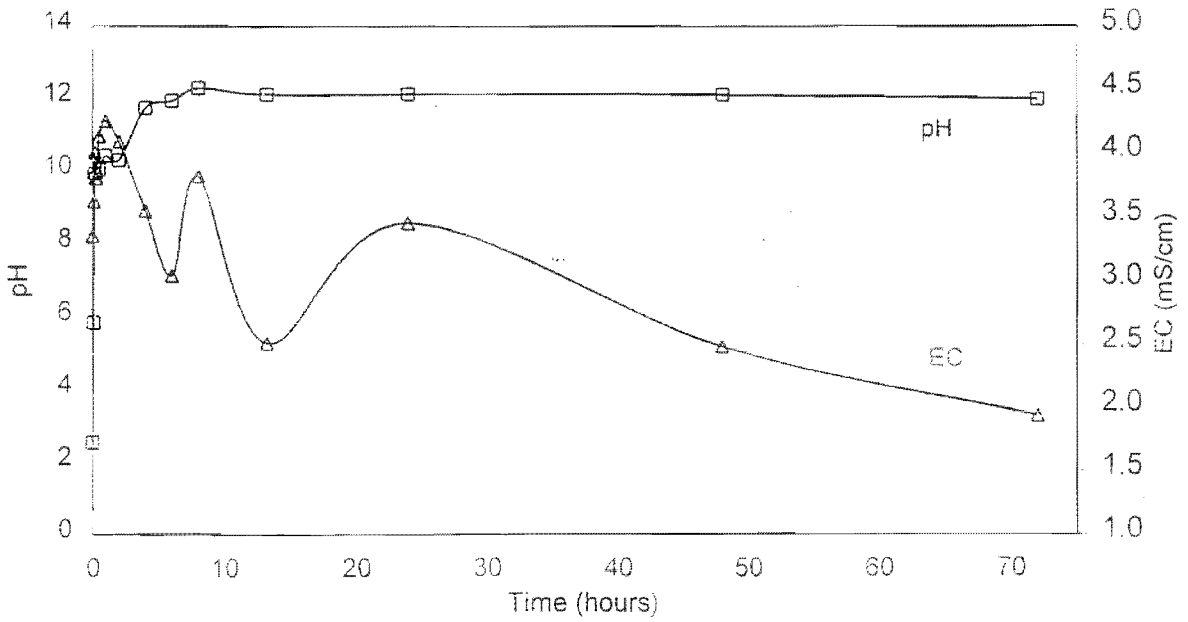

Figure 4.22: The change in pH and EC with time for Arnot fly ash at a 1:5 ratio.

The results for the 1:10 ratio of Arnot fly ash show the same trend as the 1:5 ratio, with the pH increasing rapidly before changing more slowly as a steady state is approached. The pH reaches a maximum at 10 after 8 hours, after which it decreases slowly to 9.4 after 72 hours. The EC increases rapidly to 4.1 mS/cm after 2 hours before decreasing slowly to 2.5 mS/cm after 72 hours.

The kinetics of reaction between the fly ash and AMD at a 1:20 ratio differs from the 1:5 and 1:10 ratios. The pH increased from an initial value of 2.5 to 4 within 5 minutes, after which it increased slowly reaching a maximum of pH 9.3 after 24 hours. The pH then decreased to 8.3 after 48 hours and remained stable at 8.3 until the experiment was terminated. The EC shows a small increase initially before decreasing to 3.3 mS/cm and remaining stable for the duration of the experiment.

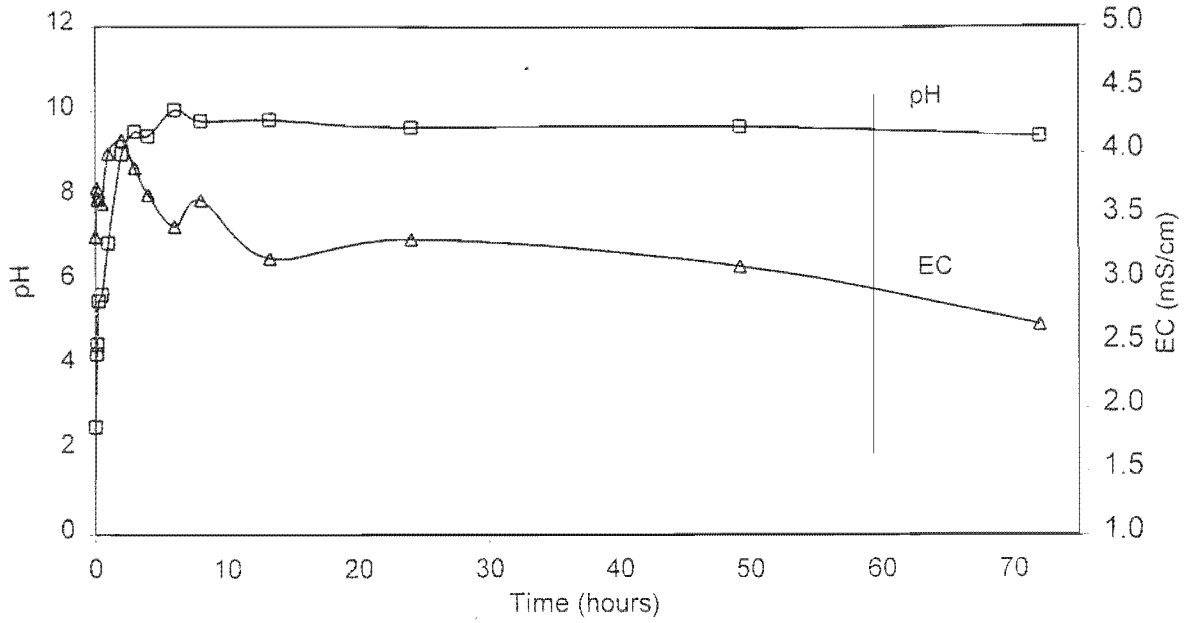

Figure 4.23: The change in pH and EC with time for Arnot fly ash at a 1:10 ratio.

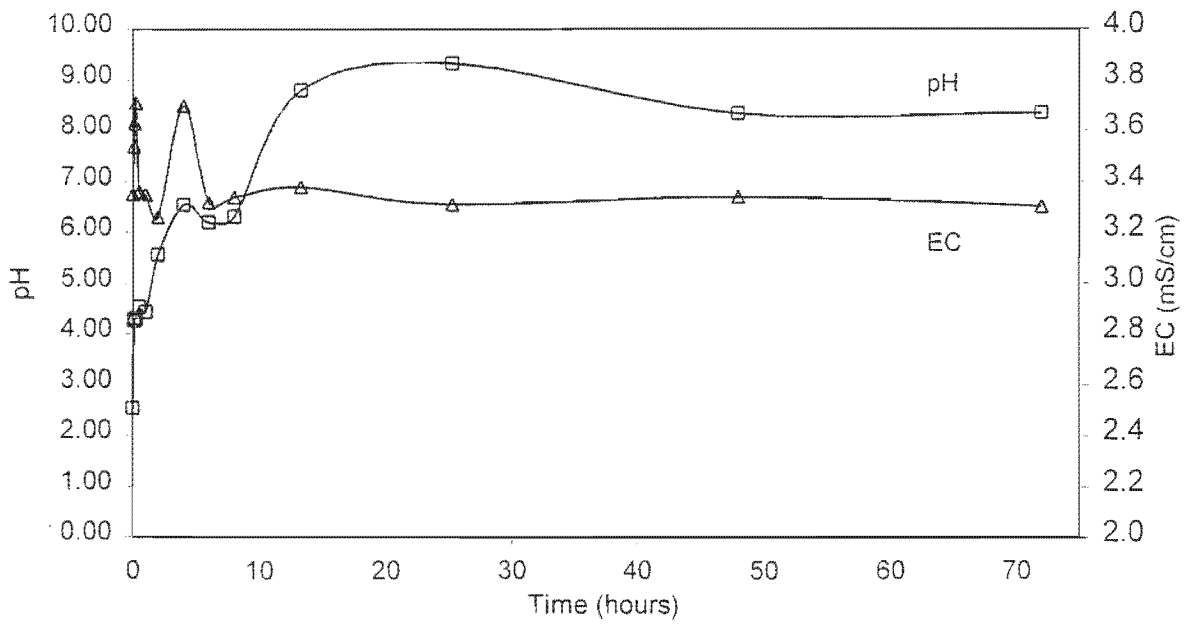

Figure 4.24: The change in pH and EC with time for Arnot fly ash at a 1:20 ratio.

4.3.2 Sasol

The kinetics of the reactions involving Sasol fly ash and AMD are presented in Figures 4.25, 4.26 and 4.27.

The reaction kinetics of the 1:5 ratio of Sasol ash and AMD (Figure 4.25) shows an increase in the pH to a value of 10 after 6 hours. The rate of pH increase then slows

down reaching a maximum pH of 11.4 after 24 hours. The pH then decreases slowly to 11.1 after 72 hours. The EC increases rapidly to 4.0 mS/cm after 15 minutes and then decreases slowly to 1.7 mS/cm at 72 hours.

The rate of pH increase for the Sasol 1:10 ratio is relatively slow reaching a value of 9.2 after 24 hours. The pH then increases slightly to a value of 9.8 before decreasing to 9.6. The EC shows a small increase during the first 2 hours before decreasing to 2.5 mS/cm after 24 hours and stabilising.

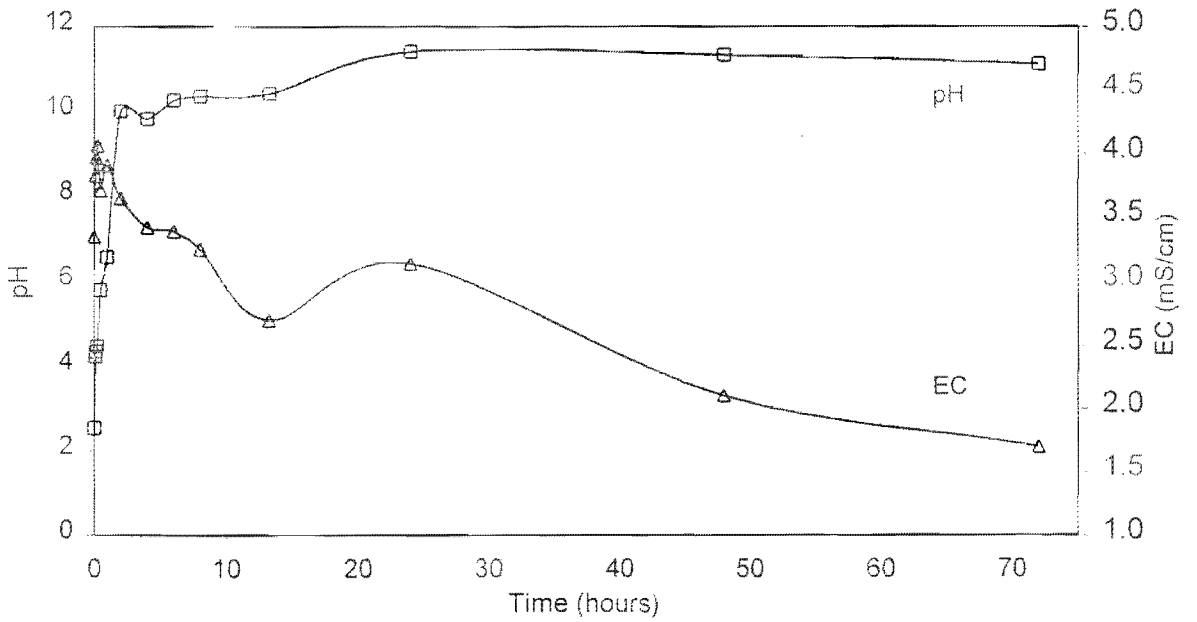

Figure 4.25: The change in pH and EC with time for Sasol fly ash at a 1:5 ratio.

The pH of the Sasol 1:20 ratio shows a slow increase to reach a maximum of 4.6 after 12 hours. The pH remains stable for the next 12 hours before stabilising at a pH of 4.4 after 48 hours. The changes in the EC follow the same trend as the pH. The EC rises slowly to a maximum of 3.3 mS/cm after 8 hours, before stabilising after 24 hours at 3.2 mS/cm.

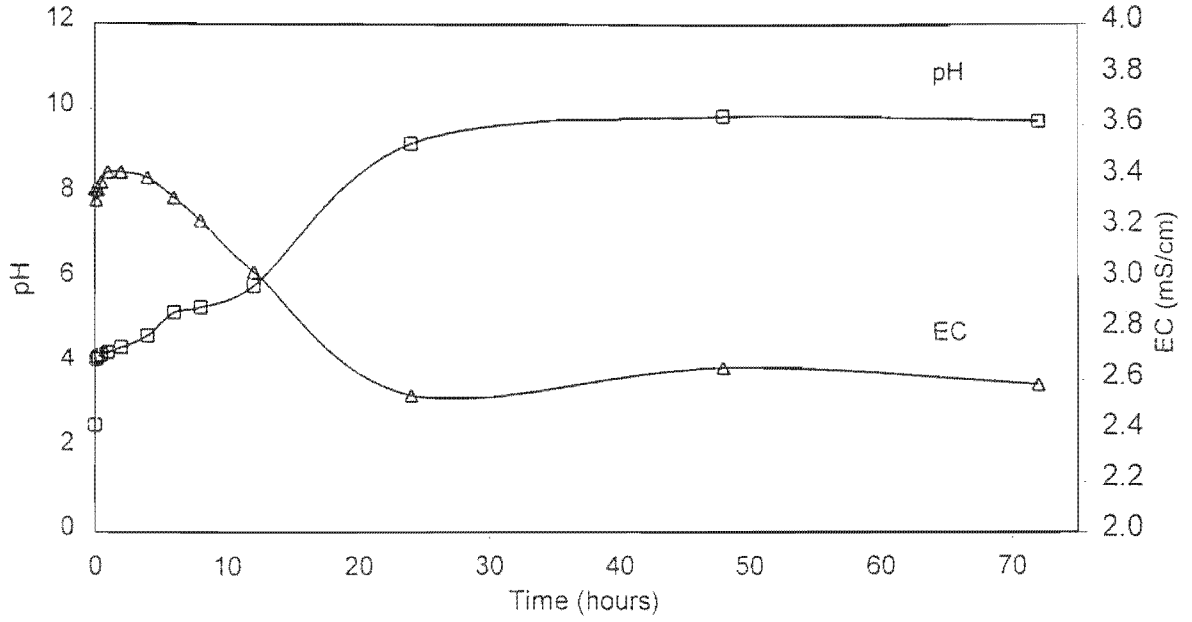

Figure 4.26: The change in pH and EC with time for Sasol fly ash at a 1:10 ratio.

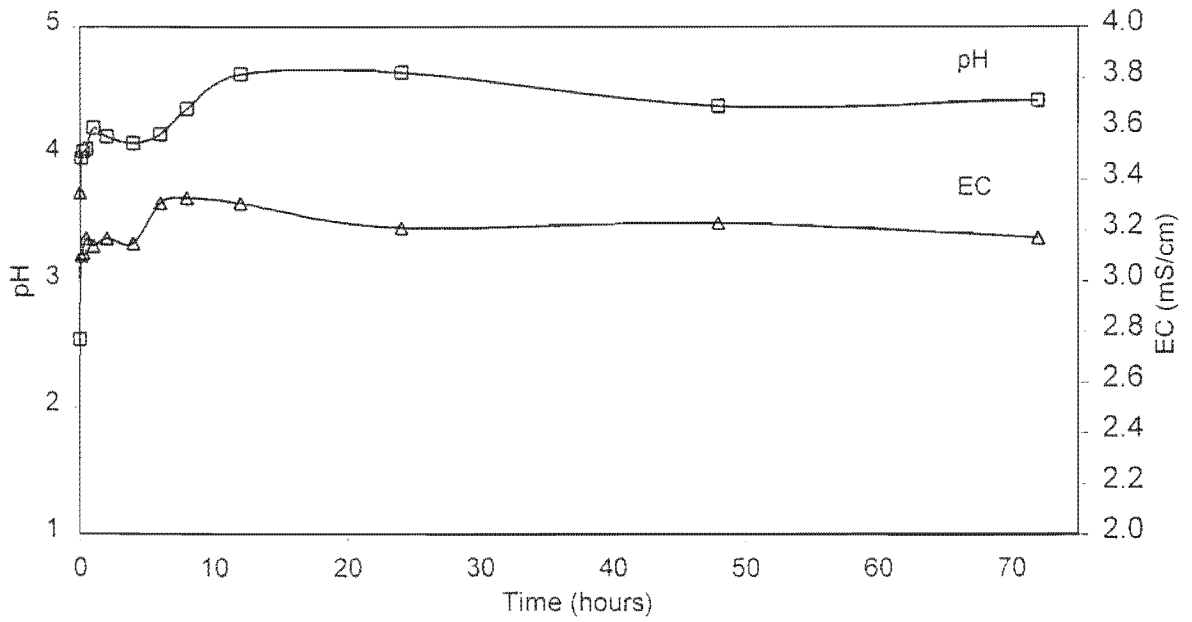

Figure 4.27: The change in pH and EC with time for Sasol fly ash at a 1:20 ratio.

4.3.3 Discussion

An inspection of the results of these kinetic experiments reveals that within the time frame of 72 hours equilibrium with respect to both pH and EC is only achieved if the equilibration pH is below pH 10. Above pH 10 the ettringite will begin to precipitate

and the slow decrease observed in the EC is most likely due to the slow kinetics of ettringite precipitation. Myneni *et al.* (1998a) found that while the onset of ettringite precipitation from supersaturated solutions was rapid, the solutions approached equilibrium relatively slowly. Slow precipitation kinetics have been observed for several mineral systems as they approach equilibrium (Oelkers *et al.*, 1994).

In all the treatments both the EC and pH showed an initial rapid increase. This rapid increase is considered to be the result of the hydration of the free lime in the fly ash. The kinetics of those treatments stabilising below pH 10 are thought to be the result of gypsum precipitation and possibly the dissolution of the glass phase.

Chapter 5:Conclusions

The CaO concentration of a fly ash is expected to have a pronounced effect on its ability to neutralise acid mine drainage. A high CaO concentration in the coal lowers the melting temperature of the coal mineral fraction, resulting in a fly ash with a more Ca rich glass and higher concentration of lime. The lower melting temperature will result in a higher concentration of aluminosilicate glass in the fly ash. The higher melting temperatures associated with low CaO coal will on the other hand promote the formation of mullite.

The Arnot fly ash with its higher concentration of lime has a larger neutralisation potential per unit mass than the Sasol fly ash. The neutralisation potential of these two fly ashes is, however, very similar above pH 10 when expressed as a function of the CaO concentration of the fresh ash. Below a pH of 10 the Arnot fly ash shows small but significantly larger ability to buffer the pH. This weak pH buffer is considered to be the result of the dissolution of the glass phase. The dissolution of the glass phase is supported by the presence of Si in the solutions. The importance of the higher mullite concentration in the Sasol fly ash is that it is less reactive than the glass phase and quartz, reducing the neutralisation potential of the aluminosilcate phases. The much weaker buffering capacity of the Sasol fly ash between pH 5 and 10 supports this.

Both the Arnot and Sasol fly ash investigated show potential for their co-disposal with AMD. The increased buffer capacity of the Arnot fly ash, at near neutral pH values, would result in their co-disposal being less prone to variations in the either the composition of the fly ash or AMD with time.

The precipitation of ettringite can result in a final effluent that has a significantly lower concentration of Ca and SO_4^{2-} than that achievable by the precipitation of gypsum. The extent to which the concentration of Ca and SO_4^{2-} is reduced will however depend on the Ca:Al:SO_4 molar ratio. If the concentration of Al is too low relative to the Ca and SO_4^{2-}, the Al will limit the formation of ettringite. The EC of the solutions for both fly ash samples show a minimum at 16.6% ash and coincides with the precipitation of ettringite. The EC achieved by the Sasol fly ash is lower than that reached by the Arnot fly ash. The concentration of SO_4^{2-} in the Arnot solution (14.6 mg/L) is however substantially less than that in the solution from Sasol (761 mg/L). The TDS of the Arnot solution (698 mg/L) is, however, lower than that of the Sasol

solution (1410 mg/L). The higher conductivity of the Arnot solution (pH 11.9) is attributed to the disproportionately large contribution of the OH^- anion to the EC. Below pH 10 the EC increases steadily, this increase is attributed to the incongruent dissolution of ettringite to gypsum and amorphous $Al(OH)_3$, resulting in a gypsiferous solution.

The fate of the trace elements present in both AMD and fly ash will be critical in determining the feasibility of their codisposal. The precipitation of ettringite could have significant implications with respect to the removal of contaminants from both the fly ash leachate and AMD. The precipitation of ettringite can also result in the attenuation of potentially harmful oxyanions such as arsenate. Arsenate can substitute for the sulphate anion in the channels of the ettringite structure. As the ettringite surface is negatively charged in this high pH environment, its ability to adsorb cationic species needs to be investigated. The coprecipitation of heavy metals with ferrihydrite is well known and can control the solubilities of these metals. The high surface area of ferrihydrite makes it ideally suited for the removal of trace metals from solution.

The mineralogy of the precipitates during the co-disposal of fly ash and AMD can be classified into three groups based on the equilibrium pH:

- Between pH values of 12 and 10 the precipitate mineralogy consists of ettringite and ferrihydrite.
- At intermediate pH values, between pH 10 and 5, the precipitates consist of a mixture of gypsum, ferrihydrite and amorphous $Al(OH)_3$.
- Below a pH of 4.5 gypsum and ferrihydrite and possibly jurbanite appear to be the stable phases.

The results of the kinetics experiments showed that for all the treatments the pH showed an initial very rapid increase. This rapid increase is considered to be the result of the hydration of the free lime in the fly ash. The onset of ettringite precipitation is rapid but the solutions approach equilibrium relatively slowly. While the slow precipitation of ettringite near equilibrium could result in higher concentrations of Ca, SO_4^{2-} and Al, the lowest EC recorded during this study corresponded with the precipitation of ettringite.

The co-disposal of these two waste products shows potential as an alternative to conventional liming practices and should to investigated further. A number of

questions remain which should to be investigated

- The fate of the heavy metals associated with AMD, particularly at pH values greater than 10.
- Expanding the study to include other fly ash from other power stations with a wider range of compositions so as to gain a better understanding of the importance of the glass phase.
- The stability of precipitates would need to be evaluated, particularly the stability of ettringite with respect to atmospheric CO_2.

6. References

Adriano, D.C., Page, A.L., Elseewi, A.A., Chang, A.C. and Straughan, I. 1980. Utilization and disposal of fly ash and other coal residues in terrestrial ecosystems: A review. Journal of Environmental Quality, 9, 333-344.

Alexander, L., and Klug, H.P. 1974. Basic aspects of x-ray absorption. Analytical Chemistry, 20, 886-889.

Allison, J.D., Brown, D.S. and Novo-Gradac, K.J. 1991. MINTEQA2, A geochemical assessment data base and test cases for environmental systems: Vers. 3.0 user's manual. Report EPA/600/3-91/-21. Athens, GA: U.S. EPA.

Atkins, M., Macphee, D., Kindness, A. and Glasser, F.P. 1991. Solubility properties of ternary and quaternary compounds in the $CaO-Al_2O_3-SO_3-H_2O$ system. Cement and Concrete Research, 21, 991-998.

Bangthanh, T., Nordstrom, D.K., Cunningham, K.M., Ball, J.W. and McCleskey, R.B. 1999. New method for the direct determination of dissolved Fe(III) concentration in acid mine waters. Environmental Science and Technology, 33, 807-813.

Bayliss, P. 1986. Quantitative analysis of sedimentary minerals by powder x-ray diffraction. Powder diffraction, 1, 37-39.

Bezuidenhout, N. 1995. Chemical and mineralogical changes associated with leachate production at Kriel power station ash dam. Unpubl. M.Sc. Thesis. University of Cape Town.

Bigham, J.M., Schwertmann, U. and Carlson, L. 1992. Mineralogy of precipitates formed by the biogeochemical oxidation of Fe(II) in mine drainage. In: Biomineralization Processes of iron and manganese. Eds. H.C.W. Skinner and R.W. Fitzpatrick. Catena Supplement 21, 219-232.

Blowes, D.W., Jambor, J.L., Hanton-Fong, C.J., Lortie, L. and Gould, W.D. 1998. Geochemical, mineralogical and microbiological characterisation of a sulphide-bearing carbonate-rich gold-mine tailings impoundment, Joutel, Québec. Applied. Geochemistry, 13, 687-705.

Bosch, G.L. 1990. The mineralogy and chemistry of pulverised fuel ash produced by three South African coal-burning power stations. Unpublished MSc Thesis, University of Cape Town, SA.

Campbell, A. 1998. Chemical, physical and mineralogical properties associated with the hardening of some South African fly ashes. Unpublished MSc thesis. University of Cape Town, SA.

Cornell, R.M. and Schwertmann, U. 1996. The iron oxides: structure, properties, reactions, occurrence and uses. VCH Publishers, Weinheim, 570p.

Diamond, S. 1983. On the glass present in low-calcium and in high calcium fly ashes. Cement and Concrete Research, 8, 1107-1113.

Drever, J.I. 1997. The geochemistry of natural waters: surface and groundwater environments. 3rd edition, Prentice-Hall, Inc.

Department of Weter Affairs and Forestry, 1995. Geohydrological assessment of old mine workings in the Blesbokspruit catchment. In: Report no. 2938/1023/1/E, Water Quality Management Series, May.

ESKOM. 1999. ESKOM environmental report.

Gazea, B., Adam, K. and Kontopoulos A. 1996. A review of passive systems for the treatment of acid mine drainage. Minerals Engineering, 9, 23-43.

Hälbich, T.F.J. 1997. The mobility of metals in acid mine drainage from abandoned coal mines. Unpublished MSc thesis. University of Cape Town, SA.

Hedin, R.S., Watzlaf, G.R. and Nairn, R.W. 1994. Passive treatment of acid mine drainage with limestone. Journal of Environmental Quality, 23, 1338-1345.

Hulett, L.D. and Weinberger, A.J. 1980. Some etching studies of the microstructure and composition of large aluminosilicate particles in fly ash from coal-burning power plants. Environmental Science and Technology, 14, 965-970.

Jambor, J.L. 1994. Mineralogy of sulphide rich tailings and their oxidation products. In: J.L. Jambor and D.W. Blowes, (Eds.) Short Course Handbook on Environmental Geochemistry of Sulphide Mine- Wastes, Mineralogical Association of Canada.

Karathanasis, A.D., Evangelou, V.P. and Thompson, Y.L. 1988. Aluminium and iron equilibria in soil solutions and surface waters of acid mine watersheds. Journal of Environmental Quality, 17, 534-543.

Lesch, W. 1987. The mineral and glass content of South African fly ash. Unpublished M.Sc. Thesis, University of Stellenbosch, SA.

Moore, A. and Taylor, H.F.W. 1970. Crystal structure of ettringite. Acta. Crystallographica, B26, 386-393.

Myeni, S.C.B, Traina, S.J. and Logan, T.J. 1998a. Ettringite solubility and geochemistry of the Ca(OH)2-Al2(SO4)3-H2O system at 1 atm pressure and 298 K. Chemical Geology, 148, 1-19.

Myneni, S.C.B., Traina, S.J., Waychunas, G.A. and Logan, T.J. 1998b. Vibrational spectroscopy of functional group chemistry and arsenate coordination in ettringite. Geochimica et Cosmochimica Acta, 62, 3499-3514.

Myneni, S.C.B., Traina, S.J., Logan, T.J. and Waychunas, G.A. 1997. Oxyanion behavior in alkaline environments: sorption and desorption of arsenate in ettringite. Environmental Science and Technology, 37, 1761-1768.

Nordstrom, D.K. 1982. The effect of sulphate on aluminium concentraions in natural waters: some stability relations in the system Al_2O_3-SO_3-H_2O at 298 K. Geochimica et Cosmochimica Acta, 46, 681-692.

Nordstrom, D.K., Jenne, E.A. and Ball, J.W. 1979. Redox equilibria of iron in acid mine waters. In: E.A. Jenne (ed.) Chemical modeling in aqueous systems: Speciation, sorption, solubility, and kinetics. American Chemical Society Symposium Series 93.

Oelkers, E.H, Schott, J. and Devidal, J. 1994. The effect of aluminium, pH, and chemical affinity on the rates of aluminosilicate dissolution reactions. Geochimica et Cosmochimica Acta, 58, 3499-3514.

Parkhurst, D.L. 1995. User's guide to PHREEQC- A computer program for speciation, reaction-path, advective-transport, and inverse geochemical calculations. U.S. Geol. Survey Water Resources Inv. Rept. 82-14.

Pulles, W., Howie, D., Otto, D. and Easton, J. 1996. A manual on mine water treatment and management practices in South Africa. Appendix Volume 1: Literature Reviews. WRC Report No 527/1/96

Reardon, E.J. 1991. An ion interaction model for the determination of chemical equilibria in cement/water systems. Cement and Concrete Research, 20, 175-192.

Rhoades, J.D. 1982. Soluble salts. pp.167-179. In: A.L. Page, R.H. Miller and D.R. Keeney (eds.). Methods of soil analysis, Part 2. American Society of Agronomy, Madison, Wisconsin.

Sasol. 1998. Sasol environmental report.

Schwertmann, U. and Fitzpatrick, R.W. 1992. Iron minerals in surface environments. In: Biomineralization Processes of iron and manganese. Eds. H.C.W. Skinner and R.W. Fitzpatrick. Catena Supplement 21, 7-30.

Singer, P.C. and Stumm, W. 1970. Acid Mine Drainage: The Rate-Determining Step. Science, 167, 1121-1123.

Smith, M.A and Harris, R.M. 1987. Fly ash disposal and utilization – environmental considerations. Ash – a valuable resource, Papers S.387, vol. 3.

Stahl, R.S., Fanning, D.S. and James, B.R. 1993. Goethite and Jarosite Precipitation from Ferrous Sulphate Solutions. Soil Science Society of America Journal, 57, 280-282.

Standard Methods. 1995. Standard methods for the examination of water and wastewater. 19th ed. American Public Health Association, Washington D.C. 1268p

Stewart, B.R., Daniels, W.L. and Jackson, M.L. 1997. Evaluation of leachate quality from codisposed coal fly ash and coal refuse. Journal of Environmental Quality, 26, 1417-1424.

Thompson, J.G. 1980. Acid mine waters in South Africa and their amelioration. Water SA, 6, 130-134.

Warren, C.J. and Dudas, M.J. 1984. Weathering processes in relation to leachate properties of alkaline fly ash. Journal of Environmental Quality, 19, 188-201.

Wesche, K. 1991. Fly ash in concrete: properties and performance. Chapman and Hall, London.

Willis, J.P. 1987. Variations in the composition of South African fly ash. Ash- a valuable resource, 2-6 February 1987, CSIR, vol. 3.

Ziemkiewicz, P.F., Skousen, J.G., Brant, D.L., Sterner, P.L. and Lovett, R.J. 1997. Acid mine drainage treatment with armoured limestone in open limestone channels. Journal of Environmental Quality, 26, 1017-1024.